Ocean Science
Discussions

EGU

5 **Title page**

FES2014 global ocean tides atlas: design and performances

Florent H. Lyard, LEGOS/CNRS, Toulouse, France / florent.lyard@legos.obs-mip.fr

Damien J. Allain, LEGOS/CNES, Toulouse, France / damien.allain@legos.obs-mip.fr

Mathilde Cancet, Noveltis, Toulouse, France / mathilde.cancet@noveltis.fr

10 Loren Carrère, CLS, Toulouse, France / lcarrere@groupcls.com

Nicolas Picot, CNES, Toulouse, France / nicolas.picot@cnes.fr

florent.lyard@legos.obs-mip.fr

https://orcid.org/0000-0001-6044-2642

Abstract

15 Since the mid-1990's, a series of FES (Finite Element Solution) global ocean tidal atlases have been produced and released with the primary objective to provide altimetry missions with tidal de-aliasing correction at the best possible accuracy. We describe the underlying hydrodynamic and data assimilation design and accuracy assessments for the FES2014 release (finalized in early 2016), especially for the altimetry de-aliasing purposes. The FES2014 atlas shows extremely significant improvements compared to the standard FES2004 and

20 (intermediary) FES2012 atlases, in all ocean compartments, especially in shelf and coastal seas, thanks to the unstructured grid flexible resolution, recent progress in the (prior to assimilation) hydrodynamic tidal solutions and use of ensemble data assimilation technique. Compared to earlier releases, the available tidal constituent's spectrum has been significantly extended, the overall resolution augmented, and additional scientific by-products such as loading and self-attraction, energy diagnostics or lowest astronomical tides have been derived from the

25 atlas and are available. Compared to the other available global ocean tidal atlases, FES2014 clearly shows improved de-aliasing performances in most of the global ocean areas and has consequently been integrated in satellite altimetry and gravimetric data processing, and adopted in recently renewed ITRF standards. It also provides very accurate open boundary tidal conditions for regional and coastal modelling.

Keywords

30 Global tides; unstructured modelling; data assimilation; satellite altimetry; de-aliasing

Declarations

All manuscripts must contain the following sections under the heading 'Declarations'.

If any of the sections are not relevant to your manuscript, please include the heading and write 'Not applicable' for that section.

35 *To be used for non-life science journals*

Ocean Science
Discussions

Open Access

EGU

5 **Funding**:

FES2014 project has been supported by CNRS and the French space agency (CNES) under grants n°131678, n°160306 and grants n°161431 (general grant framework no14026) and through the OSTST/TOSCA (INSU) scientific fundings.

Conflicts of interest/Competing interests (include appropriate disclosures):

10 none

Availability of data and material:

public access through AVISO+ CNES/NASA website

Code availability:

CECILL licence

15 **Authors' contributions** (optional: please review the submission guidelines from the journal whether statements are mandatory)

Please see the relevant sections in the submission guidelines for further information as well as various examples of wording. Please revise/customize the sample statements according to your own needs.

20

FES2014 global ocean tides atlas: design and performances

Florent H. Lyard[1], Damien J. Allain[1], Mathilde Cancet[2], Loren Carrère[3], Nicolas Picot[4]

[1]LEGOS, Observatoire Midi-Pyrénées, Toulouse, France
[2]Noveltis, Labège, France
[3]CLS, Ramonville, France
[4]CNES, Toulouse, France

Correspondence to: F. Lyard (florent.lyard@legos.obs-mip.fr)

Abstract. Since the mid-1990's, a series of Finite Element Solution (FES) global ocean tidal atlases has been produced and released with the primary objective to provide altimetry missions with tidal de-aliasing correction at the best possible accuracy. We describe the underlying hydrodynamic and data assimilation designs for the last FES2014 release (finalized in early 2016), and some accuracy assessments especially for the altimetry de-aliasing purposes. The FES2014 atlas shows extremely significant improvements compared to the FES2004 (Lyard et al. 2006) and (intermediary) FES2012 atlases, in all ocean regions, especially in shelf and coastal seas; these advances are due to the unstructured grid flexible resolution, recent progress in the (prior to assimilation) hydrodynamic tidal solutions and to the use of an ensemble data assimilation technique. Compared to earlier releases, the FES2014 available tidal constituents spectrum has been significantly extended, the overall resolution augmented; some new additional scientific by-products have been derived from the atlas and are available, including the loading and self-attraction effects, energy diagnostics or the lowest astronomical tides . Compared to the other available global ocean tidal atlases, FES2014 clearly shows improved de-aliasing performances in most of the global ocean areas. It has consequently been integrated in satellite altimetry and gravimetry data processing, and adopted in recently renewed ITRF standards. It also provides very accurate open boundary tidal conditions for regional and coastal modelling.

1 Introduction

The FES2014 global ocean atlas is the latest release of a twenty-years-long effort to improve tidal predictions needed in satellite altimetry de-aliasing. It is based on the hydrodynamic modelling of tides (T-UGOm unstructured grid model) coupled to an ensemble data assimilation code (SpEnOI). It is a very significant upgrade compared to both FES2004 (Lyard et al., 2006) and FES2012 (Stammer et al., 2014) atlases, thanks to the improvement of the assimilated data accuracy and the model performances. To some extent, FES2014 can be considered as an iterative step of the FES2012 atlas, mostly motivated by the overwhelming progress made in the hydrodynamic solutions accuracy late at the end of the FES2012 project and which could not be incorporated due to the project schedules. As it will be further mentioned in this publication, the efficiency of data assimilation increases significantly with prior solutions accuracy, and for two main reasons. First, despite a rigorous theoretical framework, data assimilation relies on strong assumptions in which the choice of the vector norm chosen to build the penalty function is critical (most commonly used nom is L_2-norm, which is consistent with Gaussian-shaped error probability density assumption and which leads to easily resolved linear systems, but also which tends to over-weight outliers in data or simulation values). Data assimilation must also be fed with quasi-empirical, partially subjective parameters, such as error covariances set on data. So while correcting prior

5 (hydrodynamic) solutions errors, it can also inject some methodologic errors in the assimilation solutions, more or less proportional to the prior distance between the observations and the numerical solutions. Second, as we use an ensemble technique to assess the prior modelling error covariances, and as those covariances will strongly dictate data assimilation innovation in model regions where assimilation data density is pretty sparse (sparse must be understood as compared to the tidal wavelength, hence being quite different in shallow water seas

10 compared to deep ocean regions), the prior hydrodynamic realism is critical to consistently propagate information from data locations (where data/prior model trade-off is actually solved) toward "remote" model regions. Therefore, considering the significant potential improvements and thanks to the financial support of CNES, decision was made to rapidly upgrade the FES2012 atlas toward the FES2014 atlas.

The FES2014 atlas denomination is quite misleading, as its final version has been delivered in early 2016. This

15 has left time to the project team to precisely assess the FES2014 accuracy and performances in altimetry data de-aliasing correction, and to make some final adjustments to guarantee the best possible quality at that time. It results in 3 available FES2014 releases. FES2014a is the first guess based on the self-attraction and loading (LSA) provided by GOT model and used for internal verification checks and then the production of the self-consistent FES2014b SAL atlases used within FES2014b altimetry assimilation data processing. It was not

20 aimed to be widely distributed or advertised. FES2014b is the first official release, and it has been made available after re-gridding from the native unstructured grid onto a regular $1/16^{th}$ degree resolution grid on AVISO+ website. The FES2014b atlas has been extended in 2019 to extend its long-period spectrum to low-frequency components by using the usual mass-conservative equilibrium tides approximation. To avoid confusion in public releases, the extended FES2014b atlas has received the FES2014c denomination.

25 The objectives of our communication are to concisely present the FES2014 atlas main construction details, the validation diagnostics and the available by-products, and not to propose a dissertation about tidal science findings based on this atlas which would lead us much too far. Consequently, in the following sections, we intend to provide to the reader synthetic information on the major ingredients of the FES2014 atlas production (hydrodynamic modelling, data processing and data selection for assimilation and validation, assimilation

30 processing), and some basic accuracy assessment overview.

2 Hydrodynamic prior solutions

One primary objective in the FES2014 atlas production is to dynamically model the ocean tides with the best possible accuracy, and to keep the data assimilation correction as limited as feasible, hence limiting the atlas dependency upon altimetry-derived data and altimetry errors (Zawadzki et al., 2018).

35 ### 2.1 T-UGOm time-stepping and frequency-domain solvers

T-UGOm is a 2D/3D unstructured grid model developed at LEGOS. It can accommodate a variety of numerical discretization (continuous and dis-continuous finite elements, finite volumes) on triangle or quadrangle elements, based on usual Navier-Stokes equation in the Boussinesq approximation, with non-hydrostatic pressure solver available. It can be used in time-stepping (TS) or frequency-domain (FD) mode. In 2005, based on FES2004

40 experience, an internal tide wave drag parameterization (ITWD) has been implemented for 2D shallow-water simulations (characterizing the energy transfer from the barotropic tides to the internal, baroclinic tides). ITWD parameterization originally developed from the pioneer work of Bell, 1975, and Baines, 1982, proved to be

Ocean Science
Discussions

5   essential in tidal and storm surges simulation accuracy, as tidal energy conversion account for about a significant portion of the total barotropic energy dissipation. Most of the critical dynamical parameters (such as bottom roughness, internal tide drag coefficient, etc...) can be non-uniformly prescribed inside the domain. Initially, the frequency-domain mode has been integrated in the original T-UGOm time-stepping code to dynamically and consistently downscale tidal boundary conditions for domain-limited, time-stepping simulations. The FD solver

10   is run for each tidal component separately. It basically assembles a frequency-domain wave equation and the solution is obtained by a simple inversion of the system. Naturally, the FD solver is based upon linearized equations, and subsequently non-linear processes require an iterative approach to converge toward the fully non-linear solutions. The number of iterations is rather limited for the major astronomical tidal components; it tends to increase when addressing compound and non-linear tides. In any case, the numerical cost of the FD solver is

15   extremely small compared to the TS solver cost (more than 1000 time smaller). In terms of solution accuracy, FD and TS solvers are quite equivalent, with of course a limited advantage to the TS solver in non-linear tides cases. Therefore, in the perspective of data assimilation using ensembles for the major ocean tides components, the ensemble members have been computed in the FD mode (details of data assimilation are described in a dedicated section of the article). Another major advantage of the FD solver reduced numerical cost is the

20   possibility to conduct a wide range of experiments in order to (globally or regionally) test numerical developments, calibrate the model parameters such as bottom friction and internal tide drag coefficients, verify bathymetry improvements, or examine loading and self-attraction consistency. It must be noticed that the optimal parameters set for the FD mode will also meet the TS mode requirements.

2.2 FD discrete equations

25   The T-UGOm FD solver is originally inspired from the CEFMO (Le Provost and Vincent,1997; Lyard et al., 2006) frequency-domain tidal model that was previously used for the FES atlases (such as FES2004). The frequency-domain tidal equations and the wave equation construction have been extensively described in the literature. Consequently, we will restrain to the main differences between the CEFMO and T-UGOm formulations. The FES2014 mesh is built on triangle elements. Various numerical discretizations for elevation

30   and currents can be defined on triangle elements, i.e. continuous or discontinuous, high or low order. Since its early releases, the FES tidal atlases mesh has been designed in terms of spatial resolution for continuous LGP2 discretization (quadratic basis functions, allowing for about 4 times more numerical nodes compared to linear LGP1). Among other available options, tidal velocities discretization is discontinuous NCP1. This choice has two major advantages: the elevation gradient discrete space is identical to the tidal currents space, and the

35   discrete momentum equation system is diagonal, easing the construction and solving of the wave equation. Tidal currents are expressed under a standard Galerkin procedure and this is one of the major differences with the CEFMO model where current were estimated at numerical integration nodes (Gauss quadrature).

2.3 TS discrete equations

    Quite similarly to the FD equation, the TS 2D shallow-water equations in T-UGOm are based on the so-called

40   generalized wave equation. Inspired from Lynch and Gray, 1977, and continuously developed since, it has been adapted to global ocean up to near-shore and estuarine numerical applications, with wetting/drying capabilities. Despite it is known to allow for pressure instability modes, the discretization used in FES2014 simulations is

5   (linear) LGP1 both for elevation and currents, for its numerical efficiency. As a matter of fact, the potential

pressure instabilities will appear only in some peculiar local mesh geometry and are easily avoided by precisely

controlling the mesh construction. From its earlier versions, T-UGOm includes an embedded, multi-levels, time

sub-cycling that allows for locally modifying the numerical time step. It is coupled to a simulation stability

control procedure, and sub-cycling is locally triggered and disabled following the need to control this stability on

10   the fly. This turns out to be a very efficient way to relax time step limitation due to CLF stability condition

(already eased by T-UGOm semi-implicit time scheme) and therefore to profit from the natural flexibility of

unstructured triangle grids.

2.4 Model grid settings

Since the first truly global ocean atlas (FES2004), the unstructured FES model mesh has been upgraded by using

15   regional patches. The main meshing difficulty consists in dealing with the shoreline details. Present databases

contain a high level of coastal details, much more than needed for a global ocean mesh, and that consequently

need to be filtered out. Reversely, it is necessary to maintain and assemble together some packets of micro-

islands that will form a macro-obstacle to the tidal propagation. Considering the tedious task of re-meshing most

of the ocean shorelines, automated tools have been developed to optimize the meshing operation. The targeted

20   resolution for coastal areas is 10 kilometers or less in terms of triangle side-length (Figure 1). The resolution has

been augmented to about 1.5 km in some specific places where coastal geometry is more challenging (such as

fjords, estuaries, straits, etc…). Special attention was paid to regions where the accuracy and the precision of the

available bathymetry are known to be adequate with higher mesh resolution, i.e. where mesh details will truly

reflect the bottom topography complexity. Reversely, minor upgrades were made in regions where the

25   bathymetry remains poorly known (such as the Patagonian and Siberian shelves). As a matter of experience,

increasing resolution in those regions would likely have a model accuracy worsening effect. An additional

constraint was to limit the hydrodynamic solver memory use to 30 Go in order to keep computation load at a

tractable level (at the time of production).

2.5 Model bathymetry

30   When dealing with tides, bathymetry remains one of the most critical parameters. Several global ocean databases

were available at the FES2014 production time (GEBCO, ETOPO, Smith&Sandwell) and their successive

releases have shown tremendous improvements during the last ten years. Unfortunately, none of those global

databases have the effective resolution nor the accuracy needed to be used directly in our global ocean tides

modelling. As for the earlier FES atlases, a composite bathymetry has been built from available global and

35   regional databases. In some cases, a regional digital terrain model (DTM) has been specifically constructed from

depth sounding and/or multi-beam data. A special treatment is applied to the Ross and Weddell seas, where the

free water column depth must be processed by substracting ice-shelf immersion to the bottom topography, using

the RTOPO1 dataset (Timmermann et al.). Many regions of the world ocean are now quite well documented in

terms of bathymetry, however two major continental shelves, namely the Patagonian shelf and the Siberian shelf,

40   do not match modern standards in any publically available database. Bathymetry selection, reconstruction and

merge is a tedious task, and quite uncertain because of the lack of independent validation data. Finally, the most

practical way to assess bathymetry changes remains the examination of the tidal solutions computed from the

5   candidate bathymetry. Naturally this is not a perfect measure of accuracy, as errors in bathymetry can compensate some other modelling errors, but so far we always found consistent results between improvements in bathymetry and tidal solutions. Thanks to the FD solver, extensive simulation testing can be performed, including the necessary re-calibration loop needed when modifying significantly the model bathymetry, even at regional extents, as earlier calibrations would contain error compensation bias.

10   **2.6 Loading and self-attraction effects**

Geometrical loading and gravitational self-attraction terms (LSA) are essential in tidal simulations, especially in global ocean tidal modelling (Hendershott, 1972). Those can be implicitly accounted for in the hydrodynamic tidal equations, but at a totally prohibitive computational cost. As rather accurate LSA atlases are available since the early 2010's, it is much more efficient to use explicit LSA in the simulations, not only for computational cost

15   reasons (non-sparse dynamical matrices in FD, expensive convolutions in LSA computation), but also because it tends to offer a relaxation toward the tidal atlases from which the LSA have been computed (actually, this is the only non-free ingredient of our "purely" hydrodynamic simulations). As some anomalies were detected in the SAL atlases deduced from FES2004, we used instead the FES99 LSA atlas atlases (Ray, 2013) to produce a first atlas version (FES2014-a), from which a new LSA atlas has been computed. As it will be mentioned in the

20   following sections, this new LSA atlas was used in the final FES2014-b release production.

2.7 FES2014 hydrodynamic (assimilation-free) solutions

Some parameters of the T-UGOm hydrodynamic model need to be calibrated in order to obtain the most accurate hydrodynamic solution, either to improve model realism or provide useful error compensation. The two main parameters to which the model is the most sensitive are the bottom friction coefficient and the internal tide drag

25   coefficient. Several simulations of the main tidal components (limited to M2, K1, S2 and O1 constituents) have been performed by extensively varying these two parameters, and each resulting simulation was compared to the altimetry and tide gauge validation databases. Figure 2 and Figure 3 show the vector differences between the TPJ1J2 (deep ocean) crossover point database and the hydrodynamic simulations of the FES2004 and FES2014 tidal models, for the M2 and K1 tidal components, respectively. Global values of vector differences are given in

30   Table 1, for the same three hydrodynamic simulations. These results clearly point out the improvement that has been achieved from the FES2004 to the FES2014 free simulations on the global ocean, with a global vector difference RMS nearly divided by a factor of three from FES2004 to FES2014 (M2 tidal component) in the deep ocean. The improvements are also very strong in the shelf regions, and for the other main tidal components. Moreover the histograms displayed in the "5.2 Validation " section indicate that the FES2014 hydrodynamic

35   solution reaches an unprecedented accuracy level, close to other global ocean models performances like GOT4.8/10 (Ray, 2013), EOT11a (Savcenko and Bosch, 2012), DTU10 (Yongcun and Andersen, 2010) or TPXO9 (Egbert and Erofeeva, 2002), which are all empirical or assimilated models.

The case of the S2 tidal components was specifically addressed, as it derives both from atmospheric and gravitational forcing. It is even more the case for the S1 tide, which originates mostly from atmospheric forcing,

40   but because the intrinsic variability of atmosphere we do consider that it must be dealt with in storm surge correction (DAC), not in ocean tidal corrections. Some other tidal constituents have a clear atmospherically-forced component (such as S1, K2 and even M2), but at a much lower level. Consequently, to insure the best

5   possible prior solution, the S2 wave was computed in the spectral domain using atmospheric pressure forcing at
       S2 frequency, based on ERA-interim 3-hour data.

3 Tidal harmonic constant data processing

       Tide gauges and altimetry-derived harmonic constant data have been used both in simulations' validation and
       data assimilation steps. Concerning the tide gauge data, preference was given to tide gauges for which the
10   original time series were available and documented, hence for which basic quality control could be performed
       throughout harmonic analysis and/or operational reports. In most cases, the time series were long enough so that
       a wide tidal spectrum could be analyzed with the best possible accuracy. To some extent, tide gauge selection
       (either for validation or data assimilation purposes) is more a question of how much representative are the tides
       captured by the instruments (especially in coastal seas) and keeping a balanced distribution all over the ocean
15   regions. Several tidal gauges databases have been used within the FES2014 project: a harmonic analysis was
       performed on time series from GLOSS (Holgate and al., 2013) and SONEL (Wöppelmannn and Marcos, 2016),
       databases, GLOSS being a global observation network and SONEL providing measurements on all French
       territories; then three validated databases provided by R. Ray have been used (Ray et al., 2013), named
       Deep_BPR, Shallow and Coastal hereafter and respectively dedicated to deep ocean, shallow waters and coastal
20   regions.
       The altimetry-derived time series show more processing and accuracy issues, with a strong dependency on the
       mission orbit and duration (which firstly determine the level of contamination of the tidal analysis by non-tidal
       ocean signal). Clearly, the twenty years and more duration of the Topex-Poseidon and Jason series on a nearly
       ten-day repeat orbit allows for deriving outstandingly high-quality along-track and cross-over datasets of tidal
25   harmonic constants. Moreover the altimetry dataset benefits from new altimeter standards, which allow a better
       observation of the tidal signals: GDR-D and REAPER orbits, ERA-INTERIM Dynamic Atmospheric Correction
       for ERS and TOPEX missions, improved wet tropospheric, sea sate bias and ionospheric corrections, and new
       mean profiles computed on a 20-year period (Carrère and Lyard, 2003; Carrere et al, 2016). TOPEX-Interleaved
       track (noted TPN-J1N) also provides an accurate crossover dataset, but still with a higher error level than the 20
30   years of TP-Jason series, due to the shorter period of 6 years available. ERS/Envisat series and GFO series do
       not have the same level of accuracy, as their orbits offer higher space coverage at the price of a lower temporal
       coverage (time sampling of 35 days for ERS/Envisat and 17 days for GFO). The time under-sampling of tidal
       observations affects the apparent tidal periods (aliasing effect) which depend on the true tidal periods and on the
       mission temporal repetitivity. Because of the red nature of the ocean energy spectra, the contamination of the
35   tidal signal by non-tidal signals will increase with the value of the aliased period. The TP/Jason orbit was
       deliberately chosen to maintain the aliased period in a reasonable range. Reversely, sun-synchronous orbits (such
       as ERS/Envisat/Altika) are disadvantageous in that matter: not only the S1 and S2 tides are projected on an
       infinite period (mean state), but many other tidal constituents show a rather large aliased period (cf Table 2).
       This would prevent us to use ERS/Envisat derived data, and concentrate only on the Topex/Jason dataset,
40   however the inclination of Topex/Jason is rather low and ERS/Envisat remains the only choice for very high
       latitudes and polar seas. Thus for the purpose of the FES2014 tide model, crossovers and along-track data from
       TOPEX/Jason-1/Jason-2 were preferred and were completed with some crossover data from TPN-J1N and ERS-

5   Envisat series in some shallow water regions and at high latitudes respectively. Table 3 presents the altimeter dataset used for the estimation of the harmonic constants within the FES2014 project.

3.1 Tidal loading effect

As the standard tidal atlases are targeting on the ocean tide component, a tidal loading correction needs to be applied on the altimeter measurements (in addition to the so-called solid earth deformation correction). In a first

10   step, the GOT4v8ac tidal loading model was applied (Ray 2013), taking into account the recent correction of the tidal geo-center motion proposed by Desai and Ray (2014). These data have been used in the data assimilation process for the preliminary version of the ocean tide model, noted FES2014a. In a second step, a new tidal loading atlas was computed from this FES2014a ocean solution, noted "FES2014a tidal loading" (cf. section 6.3). Then,18); this FES2014a tidal loading solution was used to produce a second version of the altimeter

15   dataset, which was assimilated into the final version of the tide model named FES2014b.

3.2 Non-tidal K1 signal prior removal

Due to the aliasing effect, the K1 diurnal frequency is aliased on the semi-annual frequency with the TOPEX/Jason sampling and on the annual frequency with the ERS/Envisat orbit (cf. Table 2). Annual and semi-annual signals are quite large in the ocean, and contamination of tidal analysis by non-tidal signal severe. By

20   virtue of Parceval rule, this contamination decreases with time as the square root of the recording duration. The present reference TOPEX-Jason time series benefits from 20 years of continuous measurements and allows a very accurate estimation of all tidal components including K1. However, for the TPN interleaved and the ERS orbits, the available time series are not long enough to guaranty an accurate separation of the K1 tidal signal from the semi-annual (resp. annual) ocean variability. A large portion of annual and semi-annual ocean surface

25   signal is due to the low frequency atmospheric surface pressure, and therefore is removed by applying a storm surge or inverted barometer correction. However, ocean circulation contributes also to this signal, and to tidal harmonics contamination. To tackle this issue, and then improve the K1 tidal signal observation in the TPN and ERS/Envisat records, a specific processing has been applied, consisting in removing an estimation of the ocean annual (Sa) and semi-annual (Ssa) signals prior to the analysis. This estimation is computed from the

30   GLORYS2-V1 global ocean reanalysis provided by Mercator-Ocean (Ferry et al., 2012). As shown in Figure 4, the amplitude of the correction is well above a few centimeters in some large ocean regions. A specific study (Gulf of Tonkin) was performed by examining the K1 analyzed tidal constant misfit at cross-overs (ascending track versus descending track). The ocean circulation contamination will appear as an incoherent contribution to K1, then will be different for ascending and descending tracks. The misfits consistently reduced when applying

35   the GLORYS correction, hence demonstrating its benefice in tidal analysis accuracy.

3.3 S2 tidal constituent processing

The S2 tidal constituent is challenging as it is not observable by the ERS/EnviSat sun-synchronous orbit as mentioned before. Moreover, with its 58.74-day aliasing period, the S2 tide is linked to the residual Mean Sea Level (MSL) signal visible at the same frequency for the TOPEX and Jason time series (Ablain et al. 2010); this

40   frequency thus needs a specific attention. Particularly this signal being stronger on TOPEX, several analyses have been performed using either the entire TOPEX-Jason time series or only the Jason-1/Jason-2 recent part.

5   But due to the shorter period, the estimation error is larger for the J1-J2 estimation, and the assimilated solution
     proves to be more accurate using the estimation from the entire altimeter series.

3.4 Numerical Rayleigh criterion

     When extracting a comprehensive tidal spectrum from a sea level time series, the question of frequency
     separation must be examined carefully. In the case of a continuous (i.e. uninterrupted or sparsely interrupted)
10   time series, the Rayleigh criterion is classically used to determine frequency separation and some additional
     parameterization (based on the smoothness credo, or admittances) can be implemented to ease the harmonic
     system solving. For tide gauges as well as for most of the altimetry-derived time series, the Rayleigh criterion
     will be appropriate to predict rather accurately separation performances. However, in the case of high-latitude
     altimetric time series, the seasonal sea ice cover is responsible for annually unbalanced observations, with data
15   gaps duration that can be comparable to the aliased wave frequency. In that case, it has been observed that the
     Rayleigh criterion will return over-optimistic diagnostics. This turns into an ill-defined harmonic system, and
     consequently high level of errors in the harmonic constants deduced from its solving. Neither high-latitude point-
     by-point clearing nor data dismissing were an option, the former being a gigantic task and the latter an extremely
     damageable loss of data in already poorly documented regions. Instead, we directly examined the ratio between
20   the diagonal and extra-diagonal terms in the numerical harmonic matrix, and we used an analogy with the
     Rayleigh criterion on continuous time series (and the corresponding harmonic matrix) to decide for a maximum
     ratio (extra-diagonal/diagonal) above which the frequency separation was considered deficient.

3.5 Filtering internal tide signatures

     FES2014 is a barotropic tides model and it is not aimed to include the small scales of the internal tide signals by
25   essence. Thus internal tides surface signatures have to be removed from the altimeter data prior to data
     assimilation and validation processes. New estimations of the first baroclinic wavelengths have been performed
     for the main waves M2, N2, S2, K1 and O1, using WOA2009 climatology (Locarnini et al., 2010, Antonov et
     al., 2010). They were then used to compute the along-track filtering wavelength, which is the minimum between
     twice the baroclinic wavelength and $1/15^{th}$ of the barotropic one. Figure 5 shows the filtering wavelength in km:
30   it goes to zero in near-amphidromic point areas and in shallow waters where the wavelength of the barotropic
     tide gets shorter.

4 Data assimilation

     The data assimilation method used in FES2014 is quite similar to the one used in FES2004, at the notable
     exception that the ensemble approach has been substituted to the variational one. This change in our approach,
35   initiated after FES2004 completion, is motivated by the difficulty to prescribe bathymetry errors as forcing terms
     errors, as variational technique would ask for. More generally, the ensemble technique is much more flexible and
     natural, especially when dealing with highly inhomogeneous error sources, in nature and magnitude, as it is the
     case for shelf and coastal tides.

Ocean Science
Discussions

4.1 SpEnOI assimilation code

The SpEnOI (Spectral Ensemble Optimal Interpolation) data assimilation code is an evolution of the CADOR data assimilation code (Lyard 1997, used up to FES2004), based on a variational approach using representer method, originally inspired from Bennett and MacIntosh, 1982. The main difference lies in the fact that CADOR uses a variational formulation to infer the tidal elevation error covariance matrix, using an adjoint system. If the variational approach is quite well designed to capture model errors arising from the right-hand side of the tidal equations (linear forcing terms), it turns to be poorly tractable to account for bathymetry-derived and non-linear terms (bottom friction) errors that usually dominate modelling errors in coastal and shelf seas. For these reason, an ensemble approach has been privileged to improve the realism and flexibility of the modelling errors prescriptions. The optimal interpolation denomination is an abuse as the error covariances on state vector are not academic or idealized covariances (such as Gaussian-shaped distribution), but is justified by the non-incremental nature of the data assimilation due to the frequency-domain space where it applies.

4.2 Ensembles construction

In the ensemble assimilation approach, a large number of simulations is run in order to describe the model errors. This ensemble of simulations is generated by varying the parameters and input datasets to which the model is the most sensitive. In the case of the FES2014 tidal model, the perturbations were made on the bottom friction coefficient, the tide drag coefficient, the bathymetry and the LSA. All the simulations were validated against the altimetry and the tide gauge databases, in order to identify potential outliers. In addition, the dispersion of the ensembles and the distance of the ensemble mean to the reference hydrodynamic simulation were computed, in order to verify that the ensembles were centered on the reference. In total, the whole ensemble contains 432 simulation members for each tidal constituent, built by following the methodology described in the next sections.

Perturbation of the loading tide: Numerical experiences have shown that the model is very sensitive to the explicit LSA forcing, with tidal species dependency. Namely, the diurnal tidal components (K1, O1) are improved when using the FES2012-derived LSA, while the semi-diurnal tidal components (M2, S2) are better resolved when using the FES99-derived LSA. In order to obtain a thorough description of the model errors, all the simulations based on perturbations were done twice, using the FES99 and the FES2012 loading tides as input, respectively. This doubled the number of members in the ensembles described hereinafter.

Perturbation of the bottom friction roughness: Figure 6 shows the energy dissipated by the bottom friction in the FES2014 hydrodynamic model, for the M2 tidal component. As expected, the areas where the dissipation is the largest correspond to the shelves and coastal seas. The model is consequently more sensitive to the bottom friction coefficient in these areas. Following this map, thirteen polygons, highlighted in red on Figure 6, were defined in order to generate local perturbations of the bottom friction coefficient in significant bottom friction tidal dissipation regions. For each of these polygons, the bottom friction roughness was assigned eight different values ranging around the global value set for the reference hydrodynamic simulation (10^{-3}m). As presented above, all the simulations were done twice, with the FES99 and the FES2012 loading tides respectively as input, and the ensemble of bottom friction perturbations finally contains 208 simulations.

5   **Wave drag coefficient**: Contrary to the bottom friction, the energy dissipation due to the energy transfer from the barotropic tides to the baroclinic tides (internal tide drag) does not happen in very specific and local regions, but in various, dispersed, sloppy bottom topography regions (shelf edges, ocean ridges) where the tidal currents cross the bathymetry gradients, making it difficult to isolate each single active site. In addition, energy transfer efficiency is strongly dependent on local ocean stratification, which is not precisely known in standard

10   climatology or OGCMs. The perturbations of the wave drag coefficient were consequently done at the sub-divided basin scale (equatorial/tropical, mid-latitudes and high latitudes sub-divisions), showed on Figure 7. For each of these ten regions, the non-dimensional wave drag coefficient was locally varied over seven values ranging around the global value set for the reference hydrodynamic simulation (75). The wave drag perturbations ensemble of wave drag perturbations finally contains 70 simulations.

15   **Bathymetry**: Several approaches are possible for the hydrodynamic model bathymetry perturbations such as linear combinations of various datasets or modifications in specific regions from synthetic or heterogeneous bathymetry dataset. The latter was used in the case of the FES2014 model, as it enables to better control the perturbations and to choose the most responsive regions. The reference hydrodynamic model bathymetry is replaced by depths extracted from gridone, 1 minute resolution from GEBCO and Smith&Sandwell, 15.1 release

20   in each of the 19 regions displayed on Figure 8 and chosen either for their dynamical impact on tidal solutions or for the large uncertainties on the reference bathymetry quality (such as the Patagonian shelf). However, construction of the ensemble simulations has highlighted that the two bathymetry perturbations in the Weddell Sea (polygon 6) resulted in solutions showing errors in semi-diurnal tides up to two to four times larger than the average simulations, with large increase of errors in the whole Atlantic Ocean, in the Indian Ocean and in the

25   Southern Pacific Ocean. This comes from the free water depth reduction due to the Weddell Sea ice-shelf immersion, which has been corrected in our reference bathymetry, but not in the gridone and Smith&Sandwell patches because of project schedule constraints. Despite considered as potentially critical for the model error space, Weddell region was discarded from the bathymetry patches ensemble construction, which effective set contains 36 members.

30

A few additional members have been added from the perturbations of the model minimal depth threshold. It is usually set to 10 m in the TUGO-m hydrodynamic, global ocean model. Depth threshold aims to minimize frequency-domain modelling validity limitations in very shallow waters, but more importantly to deal with the existence of unrealistically shallow depths in most bathymetry datasets. Potential errors arising from this

35   parameter has been taken into account by producing six members with global values centered around the standard value (10 m). In total, the ensemble of bathymetry perturbations contains 84 simulations (42 perturbations run with both the FES99 and FES2012 LSA).

4.3 Data selection

As described in section 3, the tide gauge and altimetry sea surface height observations were processed with a

40   harmonic analysis in order to retrieve the tidal harmonic constituents (amplitude and phase lag) for about fifteen tidal components (M2, K1, S2, O1, etc…) and the associated error estimates. The altimetry data were processed at the crossover points for the TP/J1/J2, TPN/J1N and E1/E2/EN series, and along the tracks for the TP/J1/J2 series. This means a large amount of data, with more than 9 000 crossover points for each of the TP/J1/J2 and

5   TPN/J1N series, about 64 000 crossover points for the E1/E2/EN series, and even much more points along the TP/J1/J2 tracks. In addition to severe computational cost (SpEnOI code is solving assimilation problem in the data space), the data of the whole dataset is not optimal. First TPN/J1N and E1/E2/EN data can contain errors larger than the one of the prior solution and associated error bars are not fully reliable, so their inclusion can degrade the resulting data assimilation accuracy. Second, previous studies have shown that a limited subset of

10   high-quality data can perform as well as the full dataset. Thirdly, it is the long-going objectives of FES atlases to keep the weight of data assimilation at the lowest possible level and preserve as much as feasible the hydrodynamic properties of the solutions (needed for instance to perform energy budgets). So the selection of the observations for the data assimilation process is driven by several constraints: the computing limitations in terms of memory, which are directly linked to the number of assimilated observations; the homogeneous repartition of

15   the assimilated observations all over the global ocean; the necessity to constrain more closely the model with the observations in problematic regions (i.e. where problems have been identified in the hydrodynamic solution, mostly linked with deficient bathymetry). In addition, the quality and the availability (in particular in the coastal regions) of the altimetry data are also important aspects in the selection. Actually, due to the 20 years of data available on the TP/J1/J2 orbit, the tidal constituents retrievals at the TP/J1/J2 crossover points and along the

20   tracks are more accurate than the tidal retrievals at the TPN/J1N and E1/E2/EN crossover points. However, the Topex/Jason orbit is limited to 66° in latitude, which means that the E1/E2/EN data will be needed as a complement in the high latitudes.

The altimetry assimilation dataset was built in two steps. First, a systematic decimation was performed, following the criteria detailed in Table 4. A threshold on the error estimate on the M2 tidal constituents was also

25   used as a selection criterion. As some observations will provide accurate estimate for some given tidal component and show strong error for another ones, data were then decimated specifically by applying a threshold value to the error estimate associated with the considered tidal component. In particular, regarding the S2 tidal constituent, no E1/E2/EN data were selected, because of its infinite aliasing period (sun-synchronous orbit).

30   The second step of the construction of the altimetry assimilation dataset consisted in re-ingesting TP/J1/J2 crossover and along-track data that were discarded by the spatial decimation in regions where the model needed more close constraints, using an empirical, iterative procedure. The final dataset of altimetry crossover points selected for the data assimilation process is presented on Figure 9, with a specific color for each altimetry mission. One can notice there are fewer observations in the major ocean surface circulation areas (Gulf Stream,

35   Kuroshio, Agulhas Current), because of the potentially large contamination by meso-scale dynamics. In the sub-Antarctic region, the seasonal presence of sea ice limits the availability of usable E1/E2/EN altimetry data and will be rejected by the numerical Raighley criterion at harmonic analysis step. The TP/J1/J2 along-track data, showed on Figure 10, clearly enables to densify the assimilation dataset on the shelves and near the coasts, where the amplitude of the tide and the errors of the model are the largest and tidal wavelength the shortest.

40   The tide gauge dataset for the data assimilation process was built from several initial tidal records distributions: WOCE/GLOSS coastal database, open ocean BPR database provided by R. Ray (and used as validation dataset in Stammer et al, 2015), open ocean BPR database in Antarctica compiled by LEGOS, Arctic database from Kowalik, BHI and LEGOS, and four tide gauge stations of R. Ray's shelf database, located North of Florida. The (inevitably) redundant or neighboring observations were identified and the consistency between the

5 neighbor stations was systematically verified. In total, the tide gauge database contains 600 stations (Figure 11) with a relatively homogeneous geographical repartition.

Finally, iterative data assimilation experiences proved the need for some additional observations in very peculiar regions, where neither tide gauge nor standard altimetry data were available. Dedicated coastal altimetry-derived tidal observations provided by the CTOH (TP/J1/J2) were used to better constrain the model in these specific

10 cases: 1 point North of Tierra del Fuego, 1 point in the Pamlico Bay (North Carolina) and 2 points between Southern islands of Japan. The total assimilation dataset contains 12 622 observations for the M2 tidal component and slightly less for the other components, depending on the error estimate associated with the tidal constituents or because of constituent-specific aliasing issues.

It should also be noticed that the M4 tidal component received a special treatment for the construction of the data

15 assimilation dataset. Indeed, the non-linear M4 tidal component mostly develops on the continental shelves. Because of it small amplitude in the open ocean, it is difficult to separate M4 signal from the other ocean signals with similar space and temporal scales, and the noise-to-signal ration in M4 analysis is much too large to provide appropriate data to the assimilation. Consequently, only shelves and coastal seas data have been kept from the M4 initial assimilation dataset. The complete M4 assimilation dataset contains altimetry crossover points from

20 TP/J1/J2, TPN/J1N and E1/E2/EN, along track data from TP/J1/J2, the four CTOH TP/J1/J2 coastal points previously mentioned and only one tide gauge, the Avon Mouth station, in the Bay of Bristol (UK).

5 Atlas assessment and validation

The validation of the FES2014 tidal atlas is based on a frequency-domain (harmonic) validation of the ocean tide component plus a temporal validation of the total geocentric tide component (i.e. ocean tide plus loading tide).

25 The FES2014 performances are compared to state of the art global tidal models available at the time of the study, namely GOT4v8/GOT4v10, DTU10, TPXO9v2, EOT11A and FES2012.

5.1 Description of FES2014 tidal spectrum

FES2014 is the only global tidal atlas that offers a rather comprehensive tidal spectrum of 34 tidal components, including linear components (K1, M2, N2, O1, P1, Q1, S1, S2, K2, 2N2, EPS2, J1, L2, T2, La2, Mu, Nu2, R2),

30 non-linear components (M3, M4, M6, M8, MKS2, MN4, MS4, N4, S4) and long-period components (MSf, Mf, Mm, MSqm, Mtm, Sa, Ssa). Late extension to additional equilibrium long-period tides has been recently produced. FES2014 contains either free hydrodynamics solutions or data assimilation results. The choice of the tidal components that benefited from data assimilation was made upon two criteria. First, the accuracy of the non-assimilated tidal component with regards to its amplitude: the smallest tidal components were not

35 assimilated. Second, the capability to separate the tidal components in the altimetry and tide gauge observations, in terms of signal to noise ratio: the long-period tidal components were not assimilated. Finally, the following 15 tidal components benefited from data assimilation: K1, M2, N2, O1, P1, Q1, S2, K2, 2N2, EPS2, L2, La2, Mu, Nu2 and M4. Most of the diurnal, semi-diurnal and non-linear tides were computed using the frequency-domain solver, especially the assimilated ones (for ensemble computational cost reasons). The smaller linear and non-

40 linear tidal constituents (not targeted by the data assimilation) J1, M3, M8, MKS2, N4, R2, S1, S4 and T2 were computed in time-stepping simulations, with atmospheric forcing (ERA-INTERIM) in addition to the usual tidal

5 potential forcing. No admittance relationship was used for these minor waves. The long-period components (Mf, Mm, Mtm, MSqm, MSf, Sa, Ssa) were computed in time-stepping mode without atmospheric forcing.

A major, novel interest of the FES2014 tidal atlas is the availability of many non-linear tidal constituents. These components are generally not provided by other models although their amplitudes can reach several centimeters in shallow seas and even 1 cm in the deep ocean in the case of the M4 wave. The FES2014 atlas is originally

10 designed for the tidal de-aliasing correction of the altimetry sea surface height observations, for which the mission accuracy requirements are set to 2 cm in the open ocean, so each (accurate) contribution to the tidal spectrum is of importance. Another asset of the FES2014 atlas is the supplying of six long-period tidal components (Mf, Mm, MSqm, Mtm, Sa and Ssa). These long-period components are generally approximated by the equilibrium solution in the other global ocean tidal models. At least for the constituents of period shorter than

15 one month, the overall ocean (dynamical) tide shows significant differences with equilibrium approximations. In addition, these dynamical solutions can show regional, fully unbalanced, enhancement due to topography trapped waves (for example in the Southeast Pacific). To compute the total geocentric tide, needed for altimetry observations correction, the FES2014a loading tide must be added to the FES2014b ocean tide, both being consistent as the FES2014a loading tide was removed from the altimetry data used in data assimilation step (cf

20 section 2.6).

5.2 Validation in the frequency domain

The validation in the frequency domain (i.e. of constituent harmonic constants) enables to easily identify and locate potential deficiencies in tidal atlases. The performance of the tidal model can be quite different from one region to another, but also from one tidal component to another. Such as for the hydrodynamic simulations, the

25 optimal tidal atlas (i.e. with data assimilation) has been validated by computing the vector differences between the observations (altimetry and tide gauges) for each tidal component. Figure 12 shows the vector differences between the tide gauge databases provided by R. Ray (and used as validation databases in Stammer et al, 2015) and the most recent global tidal models, for four main tidal components (M2, K1, S2 and O1). Here, it must be reminded that the deep ocean tide gauge database was included in the assimilation dataset for FES2014b. As a

30 consequence, it is expected that the vector difference between this database and the FES2014b tidal model is very low (still, it indicates that this dataset was found to be self-consistent in the data assimilation process). However, the comparison to the other databases (shelf and coastal) shows the overall excellent performance of the FES2014b tidal atlas, whatever the considered tidal component. This highlights the rather uniform accuracy of the FES2014b atlas, compared to some other competing atlases that sometimes show uneven accuracy

35 estimates, also strongly depending on the tidal constituent.

In this validation against tide gauges data, FES2014b and TPXO9 (recently released, April 2020, Egbert and Erofeeva, 2002) show the best agreement with data. TPXO9-atlas is a 1/30 degree resolution fully global solution, obtained by combining 1/6 degree base global solution TPXO.v1 and thirty 1/30 degree resolution local solutions for all coastal areas. To some extent, the regional patches in TPXO9 reproduce the (seamless)

40 FES unstructured grid flexible resolution, and therefore explain the similarities in terms of performances oin shelf and coastal seas.

Ocean Science
Discussions

Open Access

EGU

5.3 Variance reduction in satellite altimetry observations and in tidal gauges

5

A complementary validation consists in estimating the variance reduction obtained for altimeter observations or tidal gauges measurements (noted TG), when using the FES2014 tidal atlas as a correction for the barotropic tide sea surface height and comparing with other tidal atlases. This temporal approach allows taking into account the solution error as well as the omission error for the missing tidal constituents. Notice that if the geocentric tide solution is used for altimeter data, only the oceanic solution is used for tidal gauges.

10

Figure 13 shows the maps of variance reduction at tidal gauges sites from GLOSS network, when using the new FES2014b tidal model and compared to GOT4v10 solution; although some of these tidal gauges have been assimilated within FES2014 model, this diagnostic still permits to give information about the quality of the solution in coastal regions particularly on the French coasts where none data has been assimilated. Results indicate a significant variance reduction when using the new FES2014b solution compared to GOT model for nearly all sites. A few tidal gauges sites show an increased variance but these TG are located in very complex or enclosed regions and are thus not representative of the coastal ocean variability observable with a global ocean tide model. A complementary validation was performed using some independent TG along the Canadian Atlantic coasts (cf. Figure 14); it shows an important mean variance reduction of -17 cm² for the 10 TG used when using FES2014a solution instead of GOT4v10 one.

15

20

The impact of using the FES2014 tidal corrections on the global ocean is estimated by computing the altimeter SSH differences between ascending and descending tracks at crossovers, using either the new correction or a reference one. Crossover points with time lags shorter than 10 days within one cycle are selected in order to minimize the contribution of the ocean variability at each crossover location. This diagnostic allows an accurate estimation of the impact of the tide correction on the high-frequency part of the altimeter SSH. This diagnostic gives information on the temporal variance of the SSH differences in the small boxes of 4°x4° used for the computation. The analysis has been performed using several missions and many different global tidal atlases, but we will only present the results for Jason and AltiKa missions: Jason is the reference and very accurate mission and AltiKa is independent from all the models tested. Figure 15 and Figure 16 show the maps of SSH variances differences when comparing FES2014b with GOT4v10 and FES2012 tidal models. Results demonstrate a very good performances of the FES2014b tidal solution compared to the other models, with a strong variance reduction noted in all shallow water regions (more than 10 cm² when comparing to both FES2012 and GOT4v10) and also in some deep ocean areas. Statistics on AltiKa are a bit noisier compared to Jason's ones due to the shorter time series available, but they give valuable information for high latitudes: particularly FES2014a shows a strong improvement compared to FES2012 in all the Arctic Ocean region, and FES2014b also strongly reduce the variance compared to GOT4v10 in this region, except a slight raise of variance noted north of Baffin Bay when comparing to GOT model.

25

30

35

To pursue the analysis further to the coast, we consider along-track sea level anomalies (noted SLA) calculated from 1 Hz altimetric measurements. Although high-frequency signals are aliased in the lower-frequency band following the Nyquist theory application to each altimeter sampling, SLA time series contain the entire ocean variability spectrum. Figure 17 shows the difference of SLA variances when using FES2014a tide model instead of FES2012 (resp. GOT4v10) model, for AltiKa mission and as a function of distance to coast. This diagnostic shows the very strong improvement of the new tidal solution within the first 60 km from the coast on the global

40

5 ocean, with a mean variance reduction reaching more than 20 cm² within the first 30 km from the coast when comparing FES2014a and GOT models

6 FES2014 atlas additional derived products

The primary objective of the FES2014 project is to improve the tidal elevation prediction used in satellite altimetry data de-aliasing. However, additional tidal estimates are available from the modeling and data

10 assimilation outputs. Particularly, new global tidal currents maps, estimations of tidal energy budget on global ocean and loading and self-attraction components are presented here.

6.1 Tidal currents

Tidal currents have been estimated on the finite element mesh with the discontinuous P1 discretization (one estimate in the middle of each element, estimated separately for each triangle, see Figure 18). The FES2014 tidal

15 currents benefited from the data assimilation of the tidal elevations data through the dynamical correlation computed from the assimilation ensemble. The tidal currents are provided on a 1/16° grid like the elevations.

Contrary to sea surface elevation, where tides is the major contributor in most ocean regions, the validation of the tidal currents is quite challenging as it requires long-enough (several months to years) accurate current meter time series to accurately extract current harmonic constants from the tidal harmonic analysis. In addition, to be

20 useful for consistent comparisons, the current meter gauges must be moored in sites that are representative of the surrounding tidal dynamics. The main resulting constraint is to discard areas showing pronounced uneven bottom topography, as currents are highly sensitive to local bathymetry which cannot be captured properly by the model grid resolution. All these constraints (together with the fact that the access to the data is often restricted) imply that very few observations are finally available for the tidal velocities validation. Luckily, for more than

25 10 years Australia has been maintaining a network of 48 ADCP instruments all around the continent, principally through its government-supported Integrated Marine Observing System (IMOS). The Australian continental shelf has a wide range of tidal regimes ranging from macro-tidal to micro-tidal, thus providing ideal conditions to thoroughly test a model. The ADCP observations are accessible via the IMOS portal. An additional issue is that FES2014 tidal currents are representative of depth-averaged currents (as it is based on the shallow water 2D

30 equations), and currents velocity vertical profiles will potentially contain some baroclinic tidal current signal, those currents being usually one order of magnitude larger. The ADCP time series were specifically processed by CSIRO with the computation of the total currents at a mean depth, which is more comparable to currents computed with a barotropic model. Then, a harmonic analysis was performed in each current direction separately (U eastward and V northward) for five main tidal components (M2, K1, S2, O1, N2).

35 These in situ tidal harmonic constituents are compared to the FES2014 model tidal currents in terms of vector differences and tidal current ellipses characteristics differences. The latter gives a synthetic description of the tidal current for a given tidal component. Precisely, the length of the semi-major axis gives the maximum amplitude of the tidal current and the orientation of the ellipse gives the angle between the main current direction and the eastward direction. The parameters of the ellipse (orientation and lengths of the minor and major axes)

40 are computed from the tidal velocity harmonic constituents estimated in both directions (eastward and northward). The tidal current ellipses computed from the current meter observations (in red) and from the FES2014 model (in blue) are displayed for the M2 and K1 tidal components on Figure 19 and Figure 20

Ocean Science
Discussions

EGU

5   respectively. The green dots show the positions of the current meter moorings. For some moorings, the ellipses are not visible on the figures due to the very low amplitudes of the tidal currents in these micro-tidal sites. Globally, there is a very good agreement between the FES2014 model and the observations, at most of the macro-tidal sites. At some specific moorings (Darwin station and some stations inside the Great Barrier Reef), some large discrepancies are observed, that are due to the fact that these stations are very close to the coast, in

10   very shallow areas where the resolution of the FES2014 global tidal model is too coarse to accurately solve the currents. At some other stations (Coffs Harbour mooring), located in the open ocean, the model shows very strong unrealistic eastward components. This is due to a lack of resolution in the model grid, especially at the shelf break (the Coffs Harbour station is located close to a steep bathymetry slope). This is a well-known numerical artifact of the discontinuous numerical discretization of the tidal currents appearing where the model

15   grid has insufficient resolution over steep bottom topography. Somehow, the validation of the FES2014 tidal currents not only depict the overall fit with observations, but can also suggest a careful additional screening for future FES grid design, complementary to diagnostics made from the tidal elevation validation.

6.2 Energy budget

20   Barotropic tides energy budget is basically a very valuable diagnostics to examine the model performances and accuracy, and to understand more precisely how tidal dynamics works as an energy generation, transport and dissipation mechanism. It can also be a proxy of the interactions of ocean tides with ocean circulation and stratification (bottom friction and internal tides drag rates of work) and be a feeding parameter to general ocean circulation models that do not solve explicitly for the tides and need to parameterize their effects, mostly on

25   mixing. Energy budget has been estimated both from the prior, dynamically balanced tidal solutions (thanks to their unprecedented accuracy), and from the data assimilation solutions. The latter are of course more accurate in elevation and currents, but are not perfectly balanced (dynamically consistent). However the limited action of the data assimilation due to the prior solutions accuracy, and the dynamical quasi-coherence of the covariances computed from the ensembles allow for meaningful energy budget estimates.

30   Among other possible energy estimates (bottom friction, potential forces, etc... rate of work), the energy conversion rate from barotropic tides toward baroclinic internal tides (Figure 21) is very valuable diagnostic to identify and quantify internal tides generation. For example, it can be used to feed additional vertical diffusion parameterization in ocean circulation models where tides are not explicitly resolved.

6.3 Loading/self-attraction atlases

35   New maps of the loading and self-attractions effects have been estimated taking into account the preliminary FES2014a tidal elevations. In pre-FES2014 era, LSA atlases were computed from the projection of the native finite element tidal elevation upon a high resolution regular grid, either using spherical harmonics/love numbers approach or an equivalent Green function convolution. However, T-UGOm tidal models needs the gradient of LSA, obtained first through a projection back to finite element grid, then derivation. The two-ways projection

40   can trigger some undesirable numerical effects, and a new software has been developed to directly derive the LSA atlases on the finite element grid, using Green functions convolution (Lyard et al., 2020, in preparation).

Ocean Science
Discussions

5   Figure 22 shows the amplitude of the resulting M2 LSA computed from the FES2014b atlas, and the differences
     with the GOT4v8ac loading effects.

     As the computation of a tide model is an iterative process, these FES2014a LSA maps have been used to
     compute the final tidal model version FES2014b, showing an improvement of the global performances in terms
     of tidal correction as shown on Figure 23.

10   **6.4 Lowest/Highest Astronomical Tides (LAT, HAT)**

     Lowest astronomical tides are commonly used in hydrographic services as the reference level for nautical charts
     and terrain models. It is also a valuable data in maritime engineering and risk assessments studies.

     The FES2014 LAT (and HAT, highest astronomical tides) chart has been computed from an eighteen-year tidal
     prediction (to account for nodal fluctuation in tidal amplitudes) based on all available tidal constituent in the
15   FES2014 atlas (Figure 24). Mean lowest lower tides (MLLW) and mean highest higher tides (MHHW) levels (as
     used by NOAA) could be obtained in a similar way. FES2014 LAT is routinely used at LEGOS to convert
     bathymetry from hydrographic services into ocean mean-level bathymetry as needed in numerical ocean
     modelling, especially in coastal and near-shore configurations.

     7 Conclusions

20   Despite the tremendous efforts devoted worldwide to improve tidal corrections for altimetry during the last two
     decades, we still face challenging issues in shelf and coastal seas, as well as in high latitude oceans, where the
     atlases accuracy remains too limited for a precise altimetry data processing. Considering this matter, the
     FES2014 atlas can be considered as a very significant step forward, keeping close to others atlases in the deep
     ocean but showing a lot of improvements in shallow water seas, and some significant ones in the high latitude
25   seas.

     After proper, competitive evaluation procedures, it has been selected for CNES/NASA/ESA/EUMETSAT
     operational and re-processing altimetry data de-aliasing correction, and more recently as the standard correction
     in ITRF conventions. Thanks to the (accidental) unusual delay between FES2014 atlas release and this
     publication, the project team and the user's community could accumulate extensive experience on FES2014 atlas
30   performances in tidal prediction/correction domain. Namely, beside space-borne applications, it is now widely
     and successfully used for regional modelling and in situ data processing applications, supporting our confidence
     in its remarkable accuracy. As a matter of fact, one can consider that, even five years after its release, FES2014
     is well placed in the most useful global ocean tide atlases short list because of its extended tidal spectrum (34
     constituents, among which 15 were optimally adjusted by data assimilation), its unprecedented accuracy in shelf
35   and coastal seas and its coastal details grid flexibility.

     The forthcoming SWOT altimetry mission will especially profit from these specific characteristics as it will offer
     coastal and near-shore nearly continuous, high resolution coverage. However the FES project team is already
     making plans to design the next FES atlas generation, with emphasis to SWOT mission requirements and needs,
     which should be available within three years or so. Thinking about more detailed shallow water observation de-
40   tiding, the improvement of the hydrodynamic model will be one of the critical issues, and will need to aggregate
     further accurate world-wide bathymetry, which is a tedious and complicated task as the attempt to access
     national hydrographic services data is often frustrating, especially when existing data public release is limited by

Ocean Science
Discussions

5   non-scientific considerations. To some extent, we foresee that future atlases improvements and overall accuracy will be locally strongly correlated with the level of cooperation of national services in this matter. New or improved space-borne bathymetry estimates (gravimetry/sea surface inversion, IceSAT-2 laser processing, surface wave's wavelength inversion from optical data) might hopefully ease the issue, especially in remote or poorly accessible ocean parts, but open-minded international cooperation and eased public data access remain a

10   key factor for next generation tidal products. Meanwhile, we believe that FES2014 tidal atlas will remain a useful base for tidal prediction and correction, as well in terms of surface elevation and tidal currents, in present or future altimetric or gravimetric satellite observations and in many maritime applications.

References

Amante, C. and B.W. Eakins, 2009. ETOPO1 1 Arc-Minute Global Relief Model: Procedures, Data Sources and Analysis. NOAA Technical Memorandum NESDIS NGDC-24. National Geophysical Data Center, NOAA.
25   doi:10.7289/V5C8276M

Antonov, J. I., D. Seidov, T. P. Boyer, R. A. Locarnini, A. V. Mishonov, H. E. Garcia, O. K. Baranova, M. M. Zweng, and D. R. Johnson, 2010. World Ocean Atlas 2009, Volume 2: Salinity. S. Levitus, Ed. NOAA Atlas NESDIS 69, U.S. Government Printing Office, Washington, D.C., 184 pp

30

Baines, P. G., 1982: On internal tide generation models.Deep-Sea Res, 29, 307–338

Bell, T. H., 1975: Topographically induced internal waves in the open ocean.J. Geophys. Res, 80, 320–327

35   Bennett, A. F., and P. C.McIntosh, 1982: Open ocean modeling as an inverse problem: Tidal theory.J. Phys. Oceanogr, 12, 1004–1018

Carrère L. and F.Lyard, Modeling the barotropic response of the global ocean to atmospheric wind and pressure forcing – Comparisons with observations, Geophys. Res. Let., 30, 6, 1275, 2003
40

5   Carrere, L., Faugère, Y., and Ablain, M.: Major improvement of altimetry sea level estimations using pressure
    derived corrections based on ERA-Interim atmospheric reanalysis, Ocean Sci., 12, 825–842, doi:10.5194/os-12-
    825-2016 , 2016

    Desai, S. D. and R. D. Ray, "Consideration of tidal geocenter variations for satellite altimeter observations of
10 ocean tides," *Geophysical Research Letters,* 41, 2454-2459

    Egbert G. D., Erofeeva, S. Y., Efficient Inverse Modeling of Barotropic Ocean Tides, J. Atmos. Oceanic
    Technol. (2002) 19 (2): 183–204. https://doi.org/10.1175/1520-0426(2002)019<0183:EIMOBO>2.0.CO;2

15 Ferry N, Parent L, Garric G, Bricaud C, Testut CE, Le Galloudec O, Lellouche JM, Drévillon M, Greiner E,
    Barnier B, Molines JM, Jourdain N, Guinehut S, Cabanes C, Zawadzki L (2012) GLORYS2V1 global ocean
    reanalysis of the altimetric era (1993–2009) at meso scale. Mercator Ocean Quaterly Newslett 44:28–39
    DGFI-Report No.89: Savcenko R, Bosch W.: EOT11a - empirical ocean tide model from multi-mission satellite
    altimetry, 2012
20
    GEBCO Compilation Group (2020) GEBCO 2020 Grid , doi:10.5285/a29c5465-b138-234d-e053-6c86abc040b9

    Hendershott, M. C., 1972: The effects of solid earth deformation on global ocean tides.Geophys. J. Roy. Astron.
    Soc, 29, 389–402
25
    Simon J. Holgate, Andrew Matthews, Philip L. Woodworth, Lesley J. Rickards, Mark E. Tamisiea, Elizabeth
    Bradshaw, Peter R. Foden, Kathleen M. Gordon, Svetlana Jevrejeva, and Jeff Pugh (2013) New Data Systems
    and Products at the Permanent Service for Mean Sea Level. Journal of Coastal Research: Volume 29, Issue 3: pp.
    493 – 504. doi:10.2112/JCOASTRES-D-12-00175.1
30
    Le Provost C, Vincent P (1986) Some tests of precision for a finite element model of ocean tides. J. Comput.
    Phys. 65: 273-291

    Locarnini, R. A., A. V. Mishonov, J. I. Antonov, T. P. Boyer, H. E. Garcia, O. K. Baranova, M. M. Zweng, and
35 D. R. Johnson, 2010. World Ocean Atlas 2009, Volume 1: Temperature. S. Levitus, Ed. NOAA Atlas NESDIS
    68, U.S. Government Printing Office, Washington, D.C., 184 pp

    Lyard, F., 1997. Data Assimilation in a wave equation: a variational representer approach for the Grenoble Tidal
    model 10 February. J. Comput. Phys. 149 (1), 1–31. https://doi.org/10.1006/jcph.1998.5966
40
    Lyard, F., Lefevre, F., Letellier, T. *et al.* Modelling the global ocean tides: modern insights from FES2004.
    Ocean Dynamics 56, 394–415 (2006). https://doi.org/10.1007/s10236-006-0086-x

Ocean Science
Discussions

EGU

5   Lynch, D. R., Gray, W. G., A wave equation model for finite element tidal computations, DataComputers &
Fluids, ISSN: 0045-7930, Vol: 7, Issue: 3, Page: 207-228, 1979

Ray, R. D. (2013), Precise comparisons of bottom- pressure and altimetric ocean tides, *J. Geophys. Res. Oceans*,
118, 4570– 4584, doi:10.1002/jgrc.20336

10

Smith, W. H. F., and D. T. Sandwell, Global seafloor topography from satellite altimetry and ship depth
soundings, Science, v. 277, p. 1957-1962, 26 Sept., 1997

Stammer, D., et al. (2014), Accuracy assessment of global barotropic ocean tide models, *Rev. Geophys.*, 52,
15   243– 282, doi:10.1002/2014RG000450

Timmermann, R et al. (2010): A consistent dataset of Antarctic ice sheet topography, cavity geometry, and
global bathymetry. *Earth System Science Data*, 2(2), 261-273, https://doi.org/10.5194/essd-2-261-2010
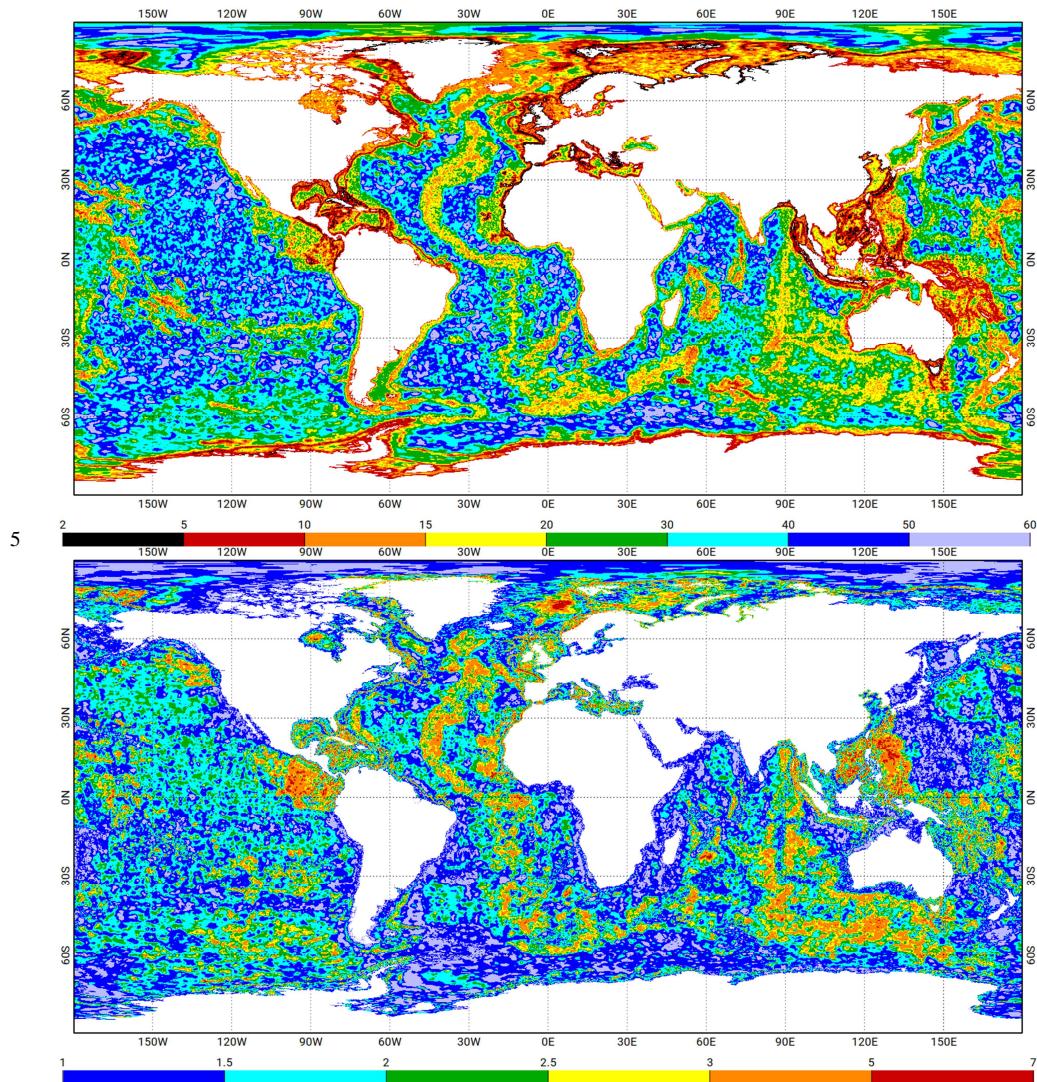
20   G. Wöppelmannn & M. Marcos (2016) : Vertical land motion as a key to understanding sea level change and
variability. Reviews of Geophysics, 54, pp. 64-92.

Yongcun Cheng, Ole Baltazar Andersen, (2010). Improvement in global ocean tide model in shallow water
regions. Poster, SV.1-68 45, OSTST, Lisbon, Oct.18-22
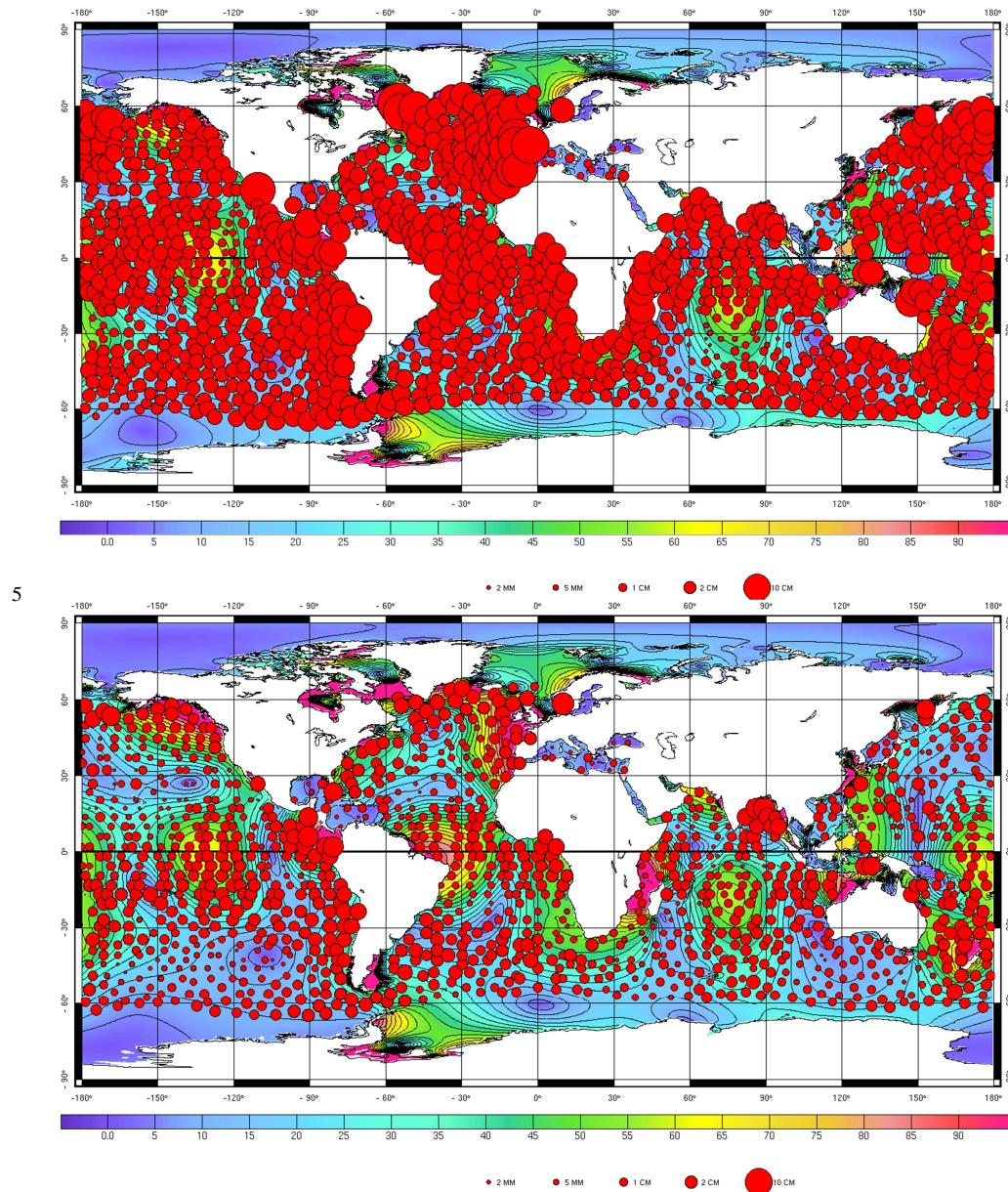
25

Zawadzki L., Ablain M., Carrere L., Ray R., Zelensky N., Lyard F., Guillot A., Picot N., (2018). Investigating
the 59-Day Error Signal in the Mean Sea Level Derived From TOPEX/Poseidon, Jason-1, and Jason-2 Data
With FES and GOT Ocean Tide Models.Ieee Transactions on Geoscience and Remote Sensing, 56, 3244-3255,
10.1109/tgrs.2018.2796630
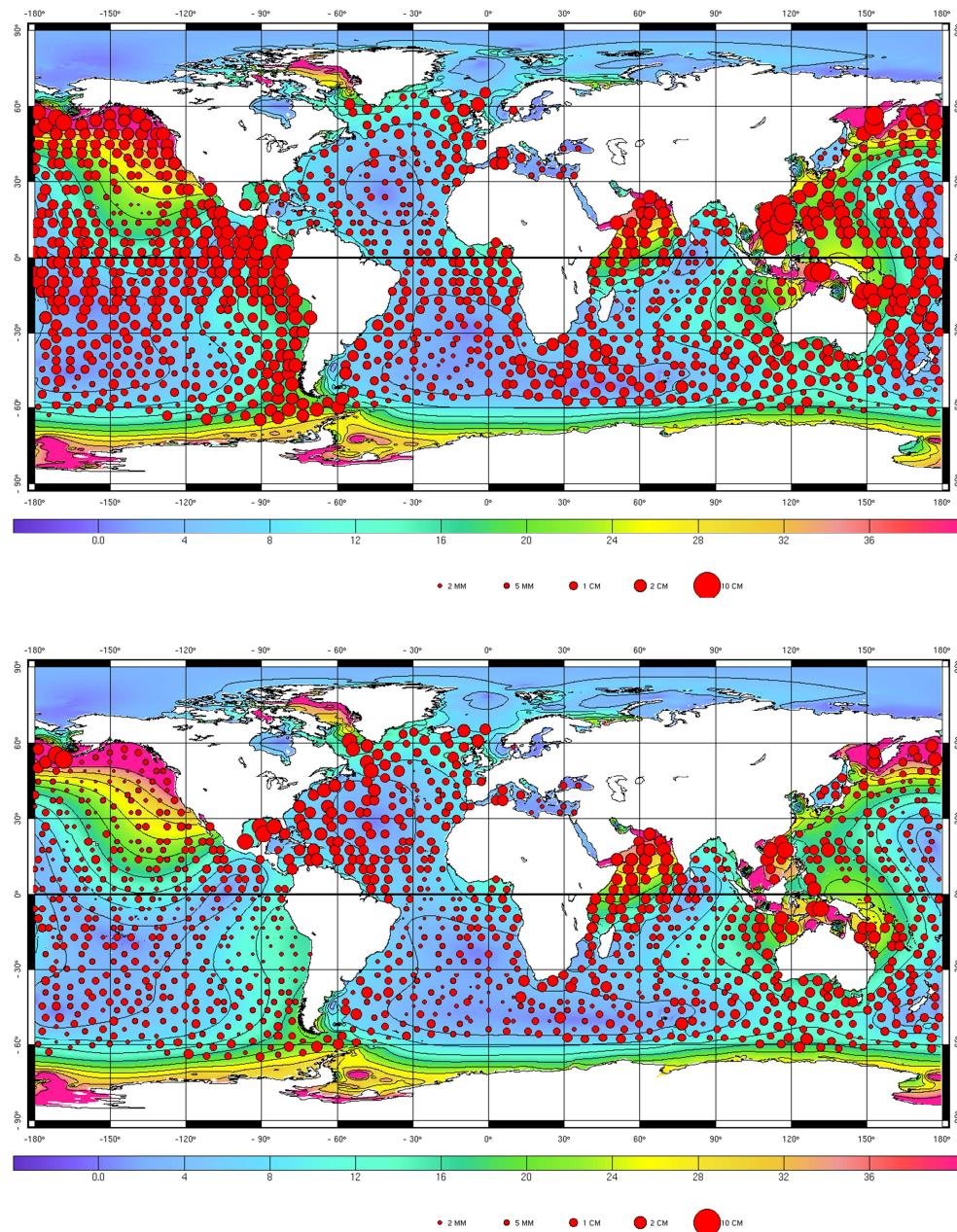
30

Figure 1: Element-wise resolution (in km) of the FES2014 unstructured grids (upper panel) and FES2014/FES2004 resolution ratio (lower panel). Resolution increase has been mostly focused on ocean ridges, shelves and shores (wherever reasonably accurate bathymetry was made available to the project). The numerical resolution of the frequency domain solutions is half the element-wise resolution due to second order basis functions (Lagrange P2).

Figure 2: Vector differences (red dots) between the purely hydrodynamic solutions of FES2004 (a), FES2012 (b) and FES2014 (c), and the deep TPJ1J2 altimeter crossover points, for the M2 tidal component. The size of the red dots is proportional to the vector difference between the model and the observations. The background colour shows the amplitude of the M2 tidal component from the model (in cm).

Figure 3 : Vector differences (red dots) between the purely hydrodynamic solutions of FES2004 (a), FES2012 (b) and FES2014 (c), and the deep TPJ1J2 altimeter crossover points, for the K1 tidal component. The size of the red dots is proportional to the vector difference between the model and the observations. The background colour shows the amplitude of the K1 tidal component from the model (in cm).

5
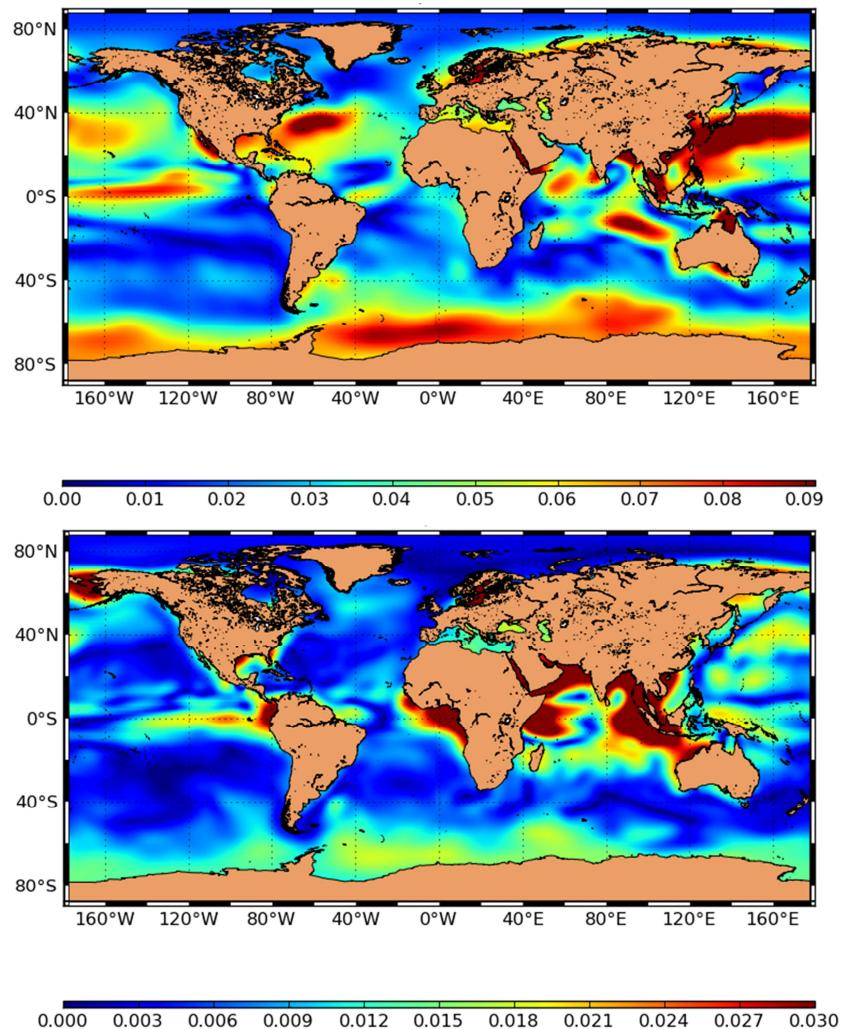
Figure 4 : maps of amplitude of Sa (upper panel) and Ssa (lower panel) ocean signals estimated from GLORYS2v1 reanalysis.

10
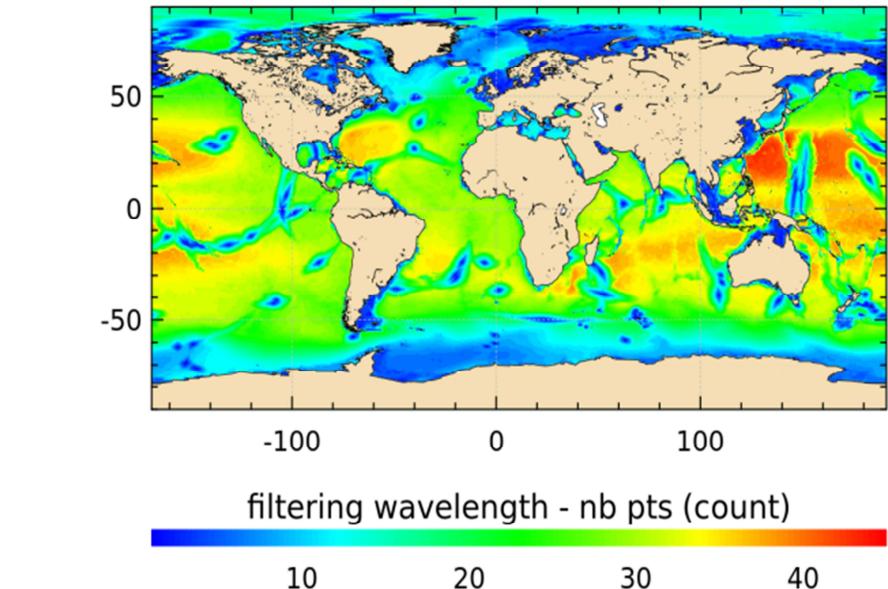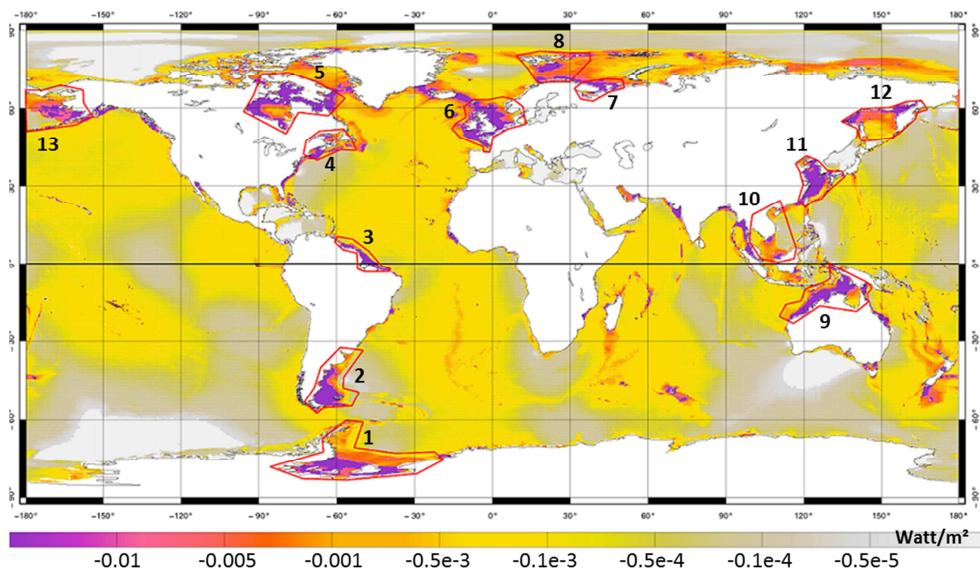
Figure 5 : along-track filtering wavelength used to remove internal tides surface signatures (in number of points)

Figure 6: Energy dissipated by the bottom friction in the FES2014 hydrodynamic model, for the M2 wave, and polygons used for the perturbations of the bottom friction coefficient.
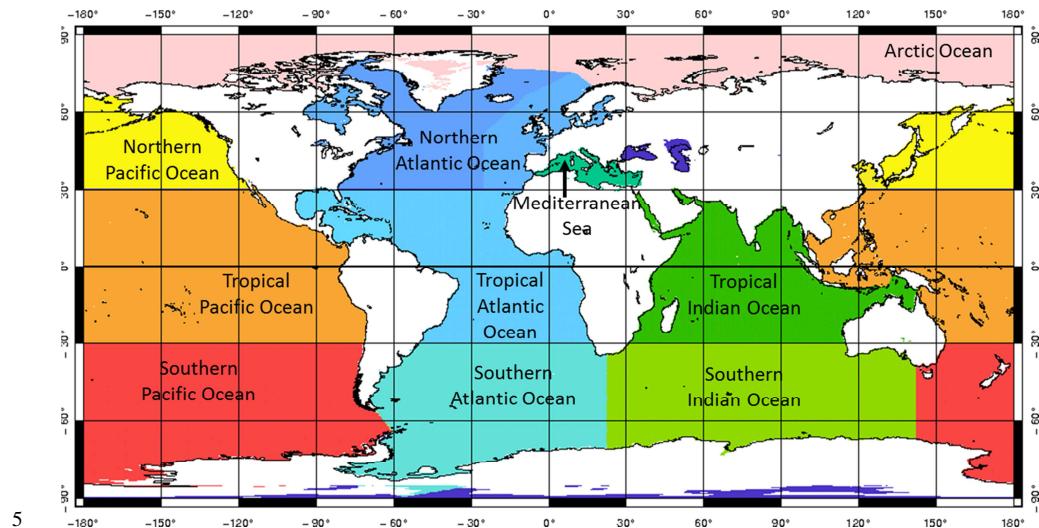
Figure 7: Division used for the perturbations of the wave drag coefficient.
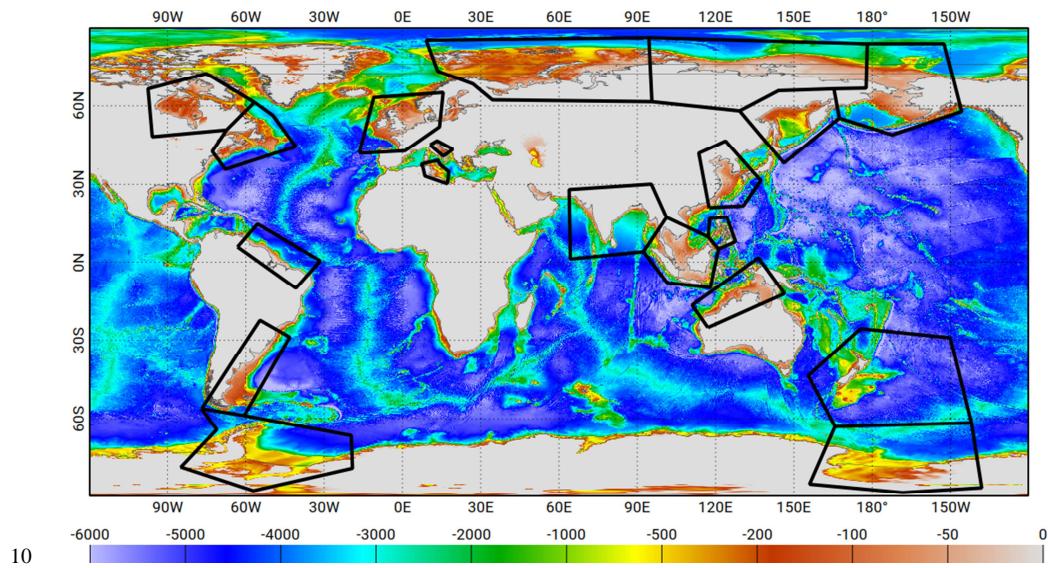
Figure 8: Bathymetry (in m) used as input in the FES2014 hydrodynamic simulation and polygons where the bathymetry perturbations were implemented for the bathymetry ensemble.

5
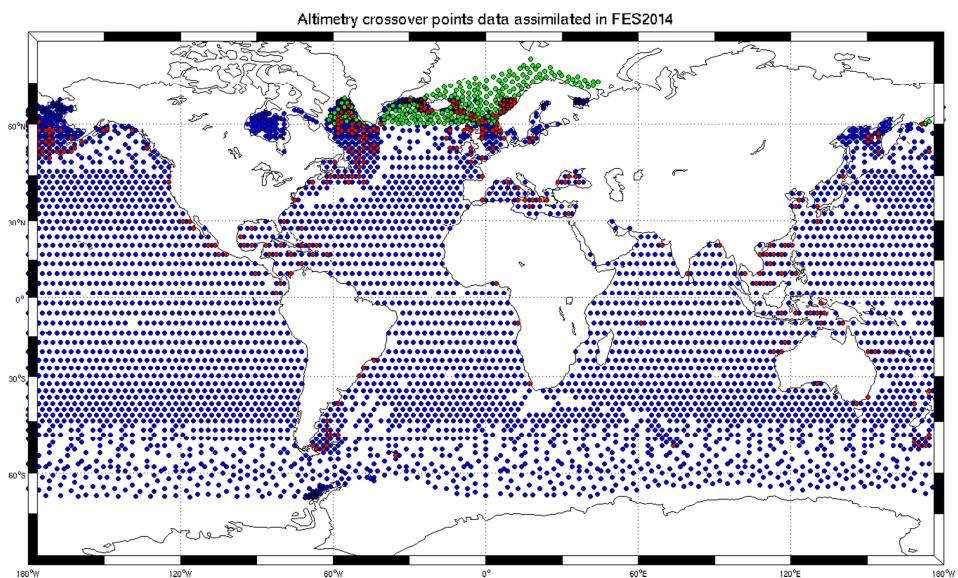
Figure 9: Altimetry crossover points selected for the data assimilation: TPJ1J2 in blue, TPNJ1N in red, E1E2EN in green.

10

5
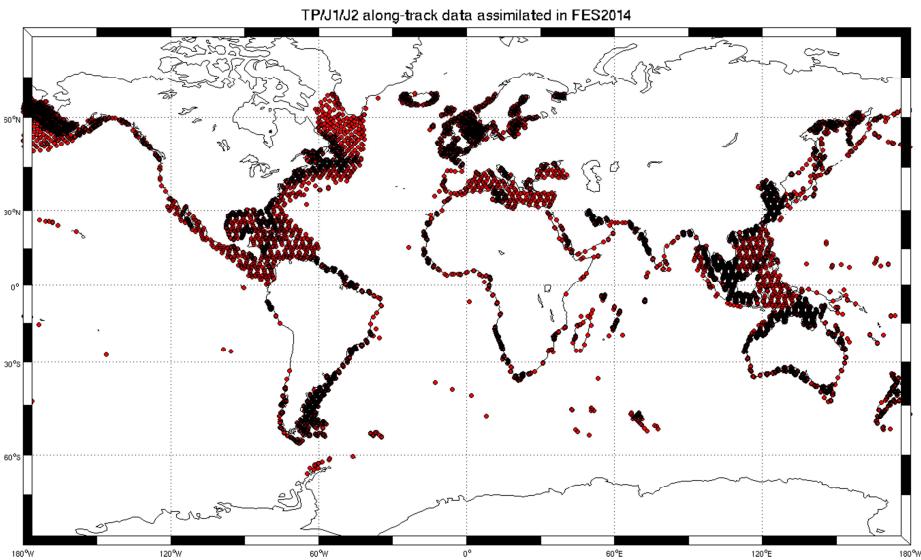
Figure 10: TP/J1/J2 along-track data selected for the data assimilation.

10
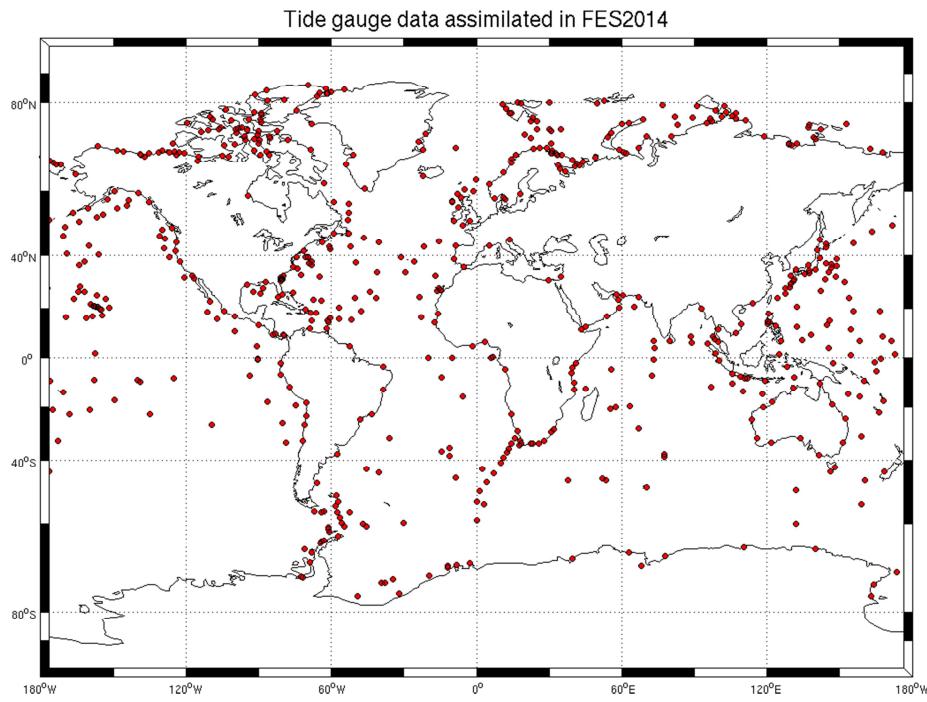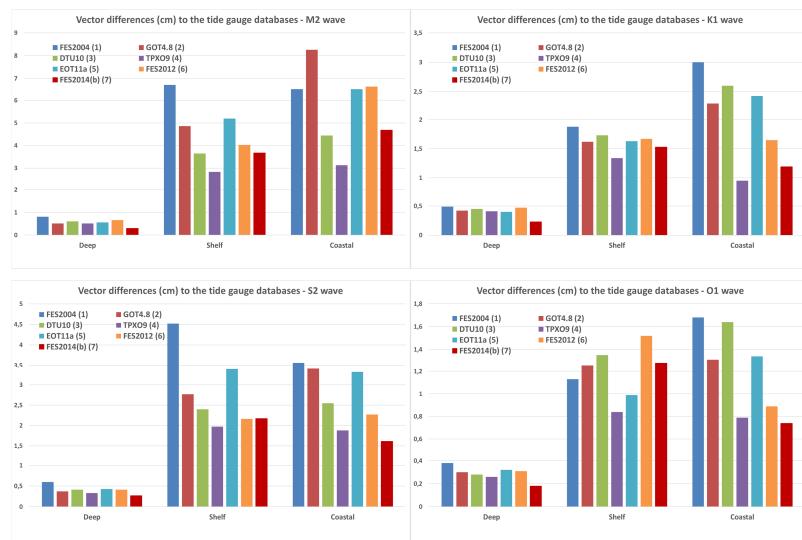
Figure 11: Tide gauge stations selected for the data assimilation

5

Figure 12: Vector differences (cm) between the tide gauge databases and the global tidal models, for M2, K1, S2 and
10 **O1.**

5
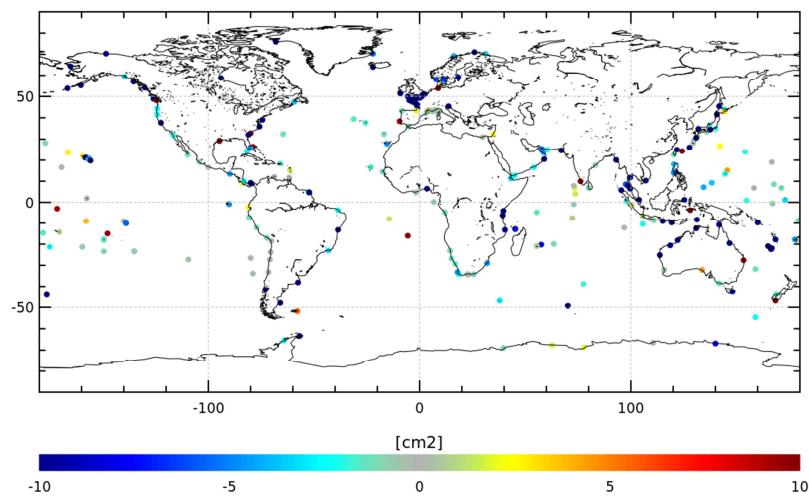
Figure 13 : Variance reduction at tidal gauges sites from GLOSS network, when using the new FES2014b tidal model and with GOT4v10 solution in cm². Analysis computed over the 2007 to 2011 time period.

10
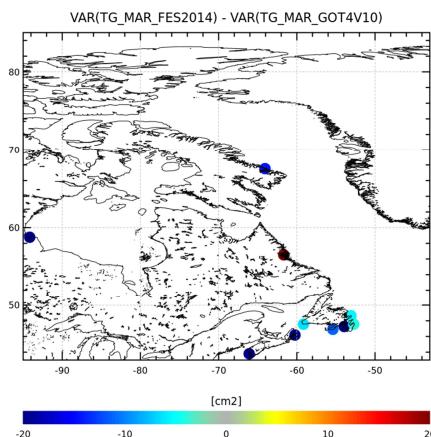
Figure 14: Variance reduction at Canadian tidal gauges sites, when using the FES2014a tidal model and compared with GOT4v10 solution in cm².
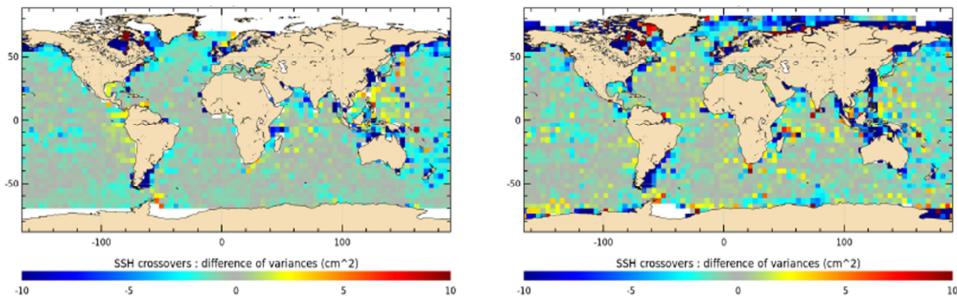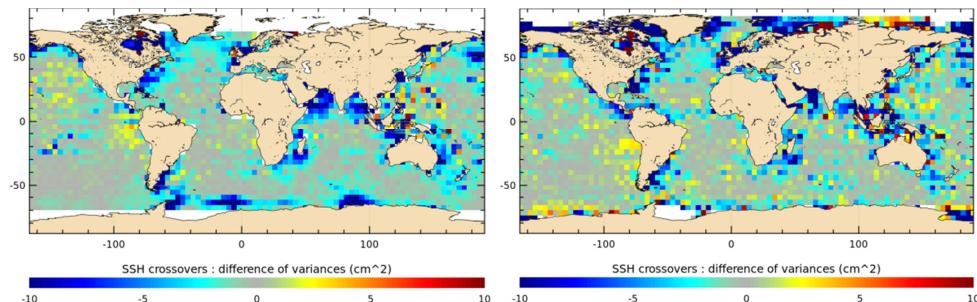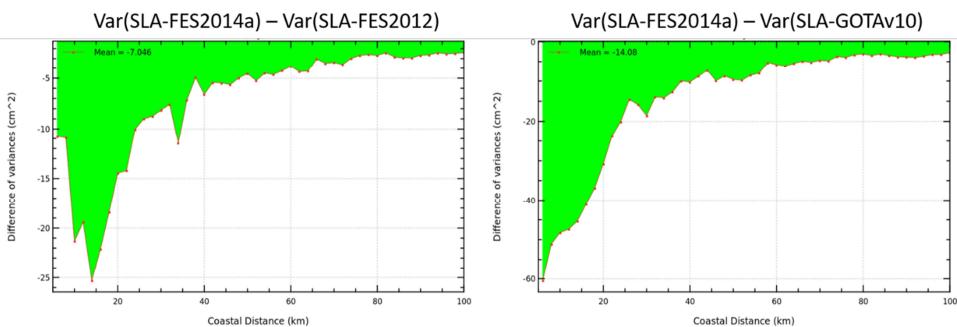
Figure 15 : maps of SSH variance differences at crossovers using either the FES2014b tidal solution or the GOT4v10 solution in the SSH calculation for Jason-2 mission (on the left, J2 cycles 1-281), and for AltiKa (on the right, AL cycles 1-21, incm²).

Figure 16 : Maps of SSH variance differences at crossovers using either the new FES2014a tidal solution and FES2012 atlas in the SSH calculation for Jason-1 mission (on the left, J1 cycles 1-248), and for AltiKa (on the right, AL cycles 1-14, in cm²).


Figure 17 : Difference of variance of SLA for AL mission as a function of distance to coast, when using the new FES2014a tide model instead of FES2012 solution (on left) or GOT4v10 solution (on right) in the SSH calculation (cm²). AL cycles 1-14 are used.

Ocean Science

Discussions

Open Access

EGU

5
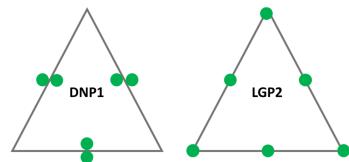
Figure 18: Principle of the DNP1 (discontinuous, non-conforming linear) and LGP2 (continuous, quadratic) discretizations used for the computation of the FES2014 tidal velocities and elevations, respectively.

10
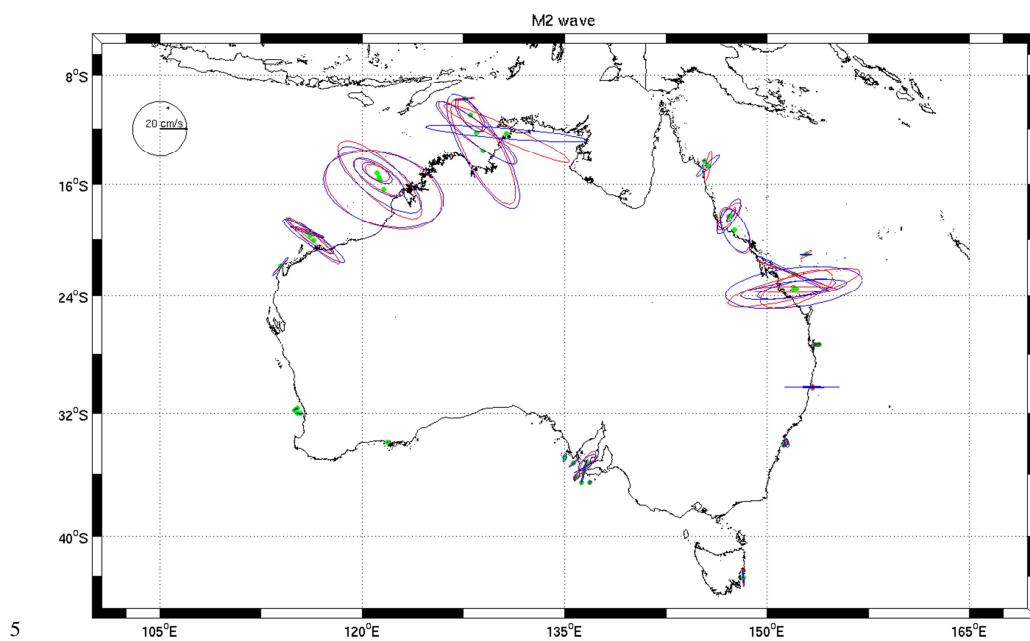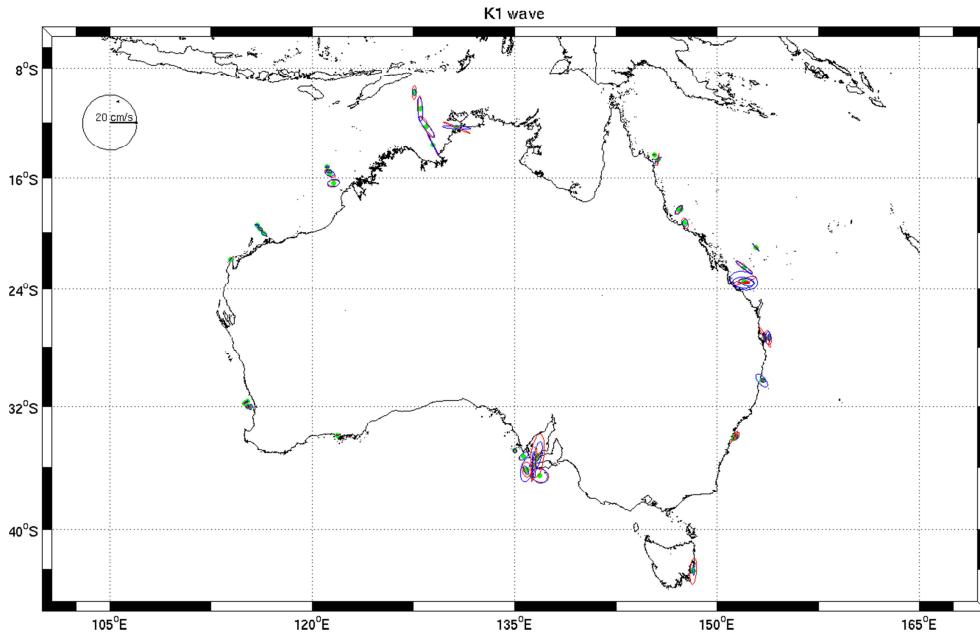
Figure 19: M2 tidal component, tidal velocity ellipses at the 48 current meter stations around Australia, for the FES2014 tidal model (blue) and the ADCP observations (red)


Figure 20: K1 tidal component, tidal velocity ellipses at the 48 current meter stations around Australia, for the FES2014 tidal model (blue) and the ADCP observations (red)

Ocean Science
Discussions

Open Access

EGU
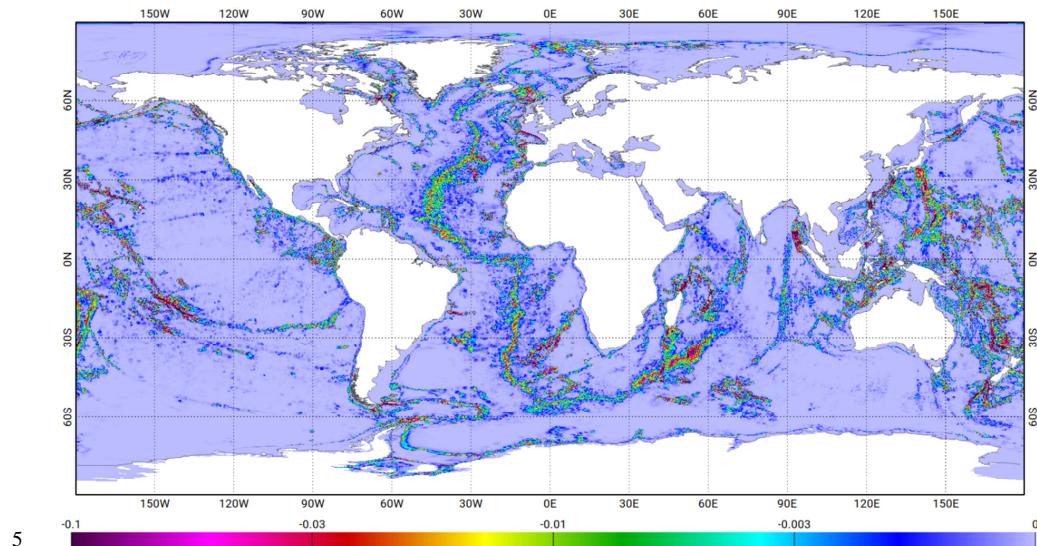
Figure 21 : M$_2$ barotropic energy conversion rate (W/m²) toward baroclinic internal tides computed from FES2014 hydrodynamic prior.

Ocean Science
Discussions

5
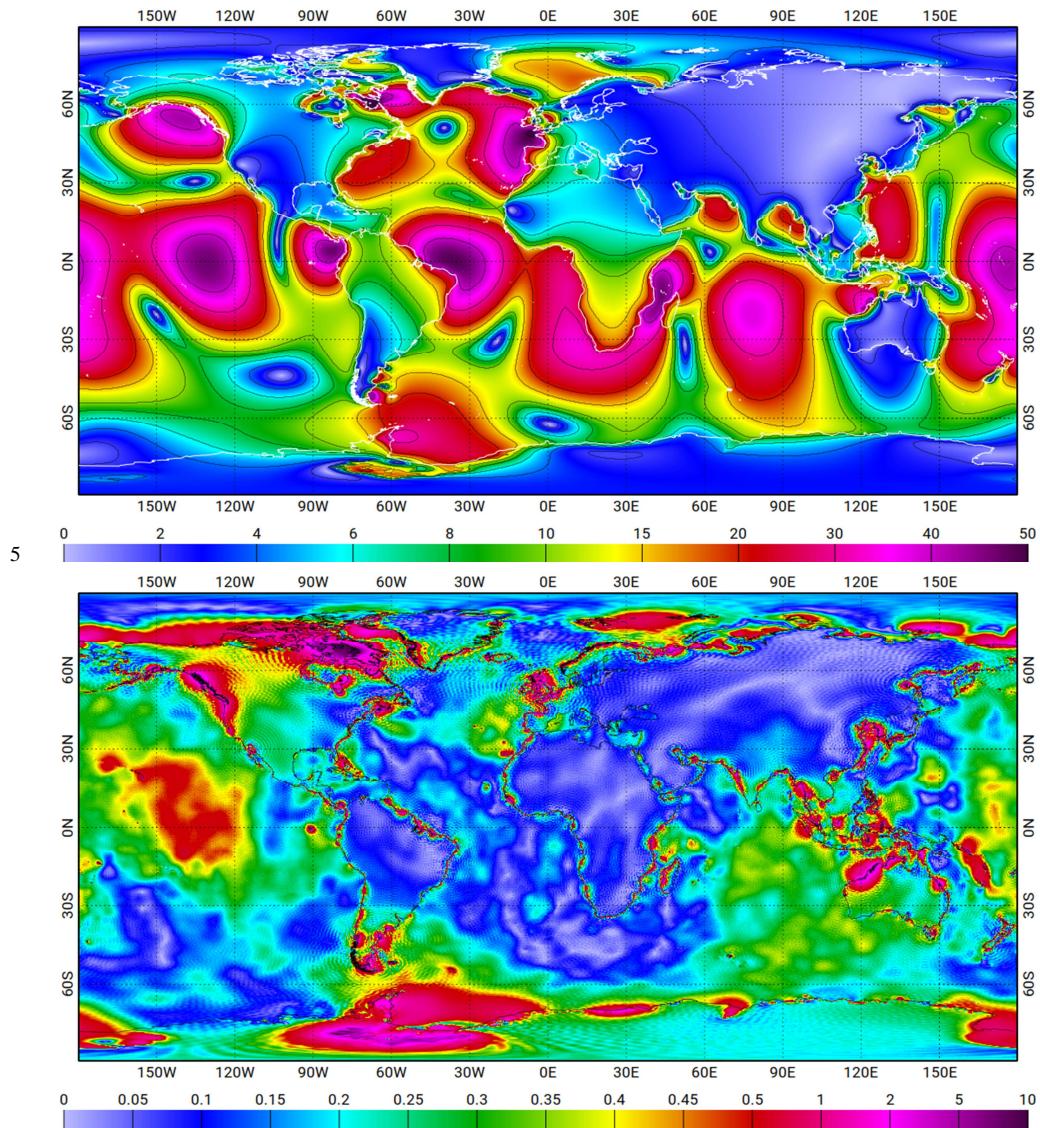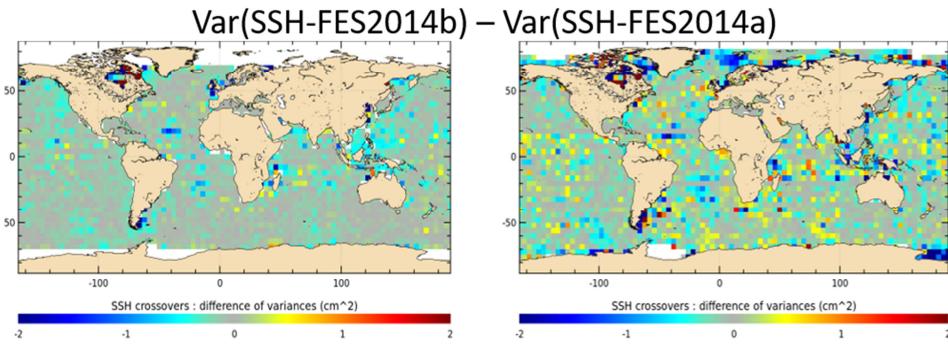
Figure 22: upper panel, M2 tidal loading, vertical displacement (cm); lower panel, M2 tidal loading vector difference between FES2014 and GOT4.10 (cm)

10

Var(SSH-FES2014b) − Var(SSH-FES2014a)

Figure 23 : Maps of SSH variance differences at crossovers using the new FES2014b tidal model or the preliminary FES2014a solution in the SSH processing for Jason-2 mission (left panel), and for AltiKa (right panel) (cm2). On one hand, FES2014b elastic tide uses FES2014a tidal loading, and on the other hand FES2014a elastic tide is based on GOT4v8ac tidal loading.
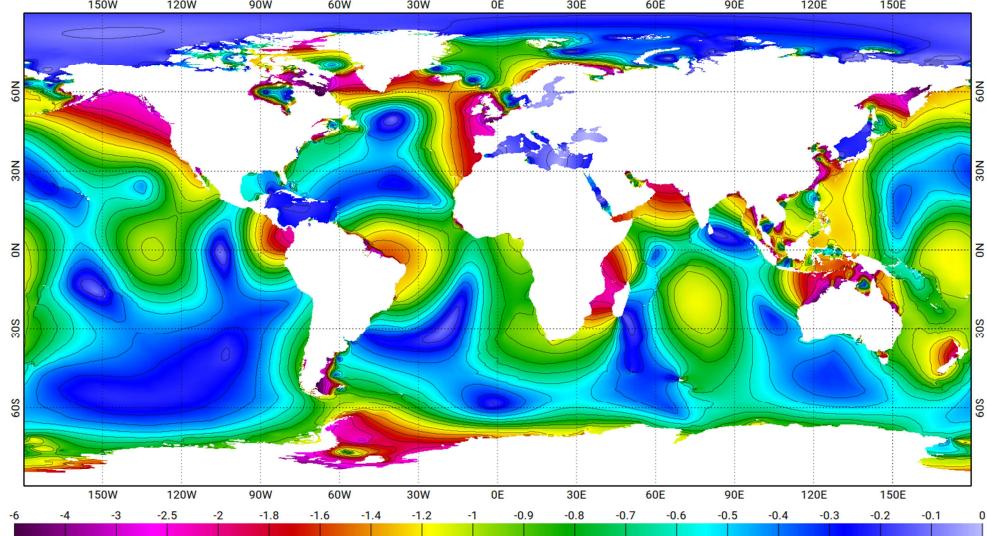


Figure 24 : Lowest Astronomical Tides (LAT) computed from an 18-year FES2014 tidal prediction.

Ocean Science

Discussions

Open Access

RMS of the vector difference (cm)	M2 tidal component		K1 tidal component	
	Xover TPJ1J2 deep	Xover TPJ1J2 shelf	Xover TPJ1J2 deep	Xover TPJ1J2 shelf
FES2004 hydrodynamic	4.56	12.32	1.45	4.19
FES2012 hydrodynamic	2.38	9.25	1.07	2.97
FES2014 hydrodynamic	1.53	6.44	0.88	2.26

5

Table 1: RMS of the vector differences (in cm) between the purely hydrodynamic solutions of FES2004, FES2012 and FES2014, and the TPJ1J2 altimeter crossover points, for the M2 and K1 tidal components.3 Tidal harmonic constant data processing

		Satellite name	T/P - Jason	GFO	ENVISAT - ERS-2
		Satellite cycle (days)	9,9156	17,0505	35
	Darwin name	Wave period	Aliasing (days)	Aliasing days)	Aliasing (days)
Long period waves	S_{sa}	182,621095	182,62109	182,6211	182,6211
	M_m	27,5545507	27,554551	44,7274	129,53
	M_f	13,6607909	36,1677	68,71484	79,92275
Diurnal waves	Q_1	1,11951486	69,364499	74,0496	132,8061
	O_1	1,0758059	45,714182	112,9535	75,06697
	P_1	1,00274543	88,89087	4466,666	365,2422
	K_1	0,99726957	173,19224	175,4479	365,2422
Semi-diurnal waves	N_2	0,52743118	49,528177	52,07205	97,39296
	M_2	0,51752505	62,107485	317,1081	94,48645
	S_2	0,5	58,741706	168,8168	#DIV/0!
	K_2	0,49863478	86,596122	87,72393	182,6211

10

Table 2 : Aliasing periods of main tidal waves for TOPEX-Jason, ERS-EN and GFO altimeter samplings

	TPJ1J2	TPNJ1N	ERS-EN
Min/Max latitude	+/- 66.14°	+/- 66.14°	80.25°N / 75.44°S
Cycle duration (days)	9.91564	9.91564	35
Number of cycles used	743	223	172

15   **Table 3 : Description of altimeter data used**

Data	Area	Resolution	Max error on M2	Nb data (M2)
TP/J1/J2 crossover points	Shelves	No decimation	1 cm	750
	Open ocean	200 km	1 cm	3677
TPN/J1N crossover points	Shelves	No decimation	2 cm	278
E1/E2/EN crossover points	Arctic Ocean	100 km	1 cm	244 *(except S2)*
TPJ1J2 along track data	Shelves	20 km	1 cm	6024

5

Table 4: Selection criteria of the altimetry observations for the data assimilation process, depending on the mission